NASA Contractor Report 182246

Liquid Droplet Generation

E. P. Muntz, M. Orme, T. Farnham, G. Pham Van Diep, P. Huerre

University of Southern California

Los Angeles, California

June 1989

Prepared for

Lewis Research Center

Under Grant NAS3-25068

Contents.

List of Figures

1 SUMMARY

A multi-stream laboratory generator was designed and fabricated in a pre-prototype configuration which would be potentially suitable for use with a Liquid Droplet Radiator. The generator was tested using two orifice arrays; one drilled by NASA Lewis, and the other fabricated by Du Pont Precision. Two fluids with viscosities of $1x10^{-5}$ m^2/s (10 cSt) and $4x10^{-5}$ m^2/s (40 cSt) were also used. Stream speeds were 10, 20, and 30 m/s. Angular dispersions of the streams from the 100 orifice Du Pont array were measured and no significant variation with stream velocity was found. The $4x10^{-5}$ m^2/s (40 cSt) fluid appears, at around $\pm 9\mu$rad, to have smaller angular dispersion than the $1x10^{-5}$ m^2/s (10 cSt) fluid. However, the resolution obtained when photographing the $4x10^{-5}$ m^2/s (40 cSt) streams was much greater than the resolution obtained when photographing the $1x10^{-5}$ m^2/s (10 cSt) streams and in retrospect there was a possibility of dissolved gases in the fluid during the 10 cSt experiments. Velocity dispersions were also measured. It was discovered that in the parameter range that was investigated, the amplitude of the disturbance applied to the stagnation cavity is an important parameter in obtaining ultra-coherent streams of droplets. It is also presumed that the more viscous fluid requires a higher power to the crystal (larger crystal deflection) than does the lower viscosity fluid, although this presumption must be verified in future investigations. The velocity dispersions for streams from several positions along the 0.13 m orifice array were similar.

A conceptual design for a 5200 stream generator was completed, incorporating ways to generate higher disturbance amplitudes than was possible in the laboratory generator. Otherwise the design is similar to that of the laboratory generator.

2 INTRODUCTION

An important application for droplet streams in space is the proposed liquid droplet radiator (LDR),[1] which would operate by employing a large number of free-flying droplet streams as the radiating element of a heat rejection system for high power space stations. A number of techniques for generating droplet streams have been considered[2]. The method

of drop generation which is implemented here is the breakup of a 100 μm diameter capillary jet into uniformly separated drops by applying a periodic surface displacement. This study is focused on the design of a multi-stream generator which is a module in a pre-prototype flight configuration for use with the LDR. It was designed such that an arbitrary number of modules can be joined together to produce the required number of droplet streams for the LDR. For example, in order to radiate 10^6 W of thermal energy, about 10^6 droplet streams are required.

To maintain efficiency in the proposed applications, it is desirable that droplet collisions are minimal, which is realized if the streams of free-flying liquid drops remain parallel, and the droplets within each stream remain unagglomerated for the duration of their flight. Both issues of stream parallelism and droplet separation are addressed in the design. The prevention of intra-stream droplet agglomeration depends on maintaining the uniformity of the intra-stream droplet separation over the flight distance and is largely dependent on the form of the disturbance applied to the stream. A new method of droplet generation, which increases the uniformity of the droplets by up to an order of magnitude compared to the conventional modes of droplet generation, is implemented in the design. Both the new and conventional modes of droplet stream production will be described in Section 3.

Stream parallelism is largely a matter of precision manufacturing and hardware design. The intrinsic directional stability of a single stream is high, having been measured to be typically around $\pm 2\mu$rad. This is illustrated by the results shown in Figures 1 and 2. The results were obtained by positioning the magnified image of the droplet stream onto a slit which was parallel to the stream's axis and just in front of a photomultiplier tube. The slit height was arranged to be approximately equal to the diameter of a magnified droplet image while its width was much less. In Figure 1, the droplet images were centered on the slit. In Figure 2, the edges of the droplet images were positioned close to the slit. The fluctuating amplitudes of the droplet signals as seen in Figure 2 compared to Figure 1 give a very sensitive indication of the position of each droplet [10,11] and give, in this case, an angular dispersion of $\pm 1\mu$rad. The stream parallelism is thus primarily dependent on the parallelism of the nozzle arrays from which the streams are generated, on nozzle exit surface

wetting, on deflections of the orifice plate, and on nozzle clogging.

The report is organized in seven major parts which follow the framework of the contract. Section 3 gives some background concerning the fluid mechanics, jet instability and multi-stream droplet sheets. Section 4 deals with the design of the generator, including considerations such as: methods of applying radial stream disturbances, eliminating angular deflection of the array when subjected to the maximum load required, eliminating angular twist of the array which may result if the surface of the array is not seated properly in the generator, and the working fluid selection. Section 5 is concerned with the fabrication of the generator. Section 6 describes the performance, testing and results for the generator operating at specified conditions. Section 7 describes the results of an acoustic analysis which deals with the generation of stagnation chamber pressure disturbances from nozzle motion, and Section 8 deals with the large scale generator design and describes the accompanying conceptual design drawings. Finally, a summary of the work done, results obtained, and areas in need of further investigation follow in Section 9.

3 JET INSTABILITY AND MULTI-STREAM DROPLET SHEETS

In this section the consequences of the droplet speed dispersion observed in the generation of droplets from capillary streams are reviewed. Droplet speed dispersion affects intra-stream agglomeration of droplets. Also, the requirements placed on a generator by attempting to minimize inter-stream collisions due to lack of parallelism are described.

3.1 Intra-Stream Agglomeration

Typically, a controlled instability of a fluid stream is introduced by disturbing the stream's surface with a sinusoidal waveform. Plateau[3] and Savart[4] were the first to observe that when a fluid stream is periodically disturbed, the stream breaks into a series of equally spaced droplets which are separated a distance corresponding to the wavelength of the disturbance. Lord Rayleigh[5] developed the linear stability analysis of the unstable jet and found that the disturbance on the stream will be unstable, and break into drops if the wavenumber of the disturbance is greater than the stream circumference. He showed that the surface waves

grow exponentially in time as $e^{\beta t}$, where β is the amplification factor. He showed further the maximum amplification factor occurred at a nondimensional wavenumber (which is the wavenumber of the disturbance multiplied by the radius of the jet) of 0.697 for an inviscid fluid. Subsequent to the analysis of Rayleigh, there has been a rich development of linear and nonlinear theories which describe the instabilities of the surface waves along with careful experiments investigating jet instabilities[6,7,8]. Most of the theories, with the exception of Chaudhary and Redekopp[9] , address the same problem: the response of a stream to imposed sinusoidal oscillations. Most of the experiments have addressed the problem of the breakup distance and the corresponding breakup time of a fluid stream when the stream is perturbed with a sinusoidal disturbance and injected into atmospheric conditions.

Chaudhary and Redekopp imposed on the stream a sinusoidal disturbance with an added harmonic, in order to suppress satellite occurrences. Satellite drops are smaller drops which may appear in-between the main drops and result from nonlinearities in the breakup process. For the application of ink jet printing, the occurrence of satellite drops is very undesirable.

Two of the present authors have recently discovered [10] a new disturbance waveform that dramatically improves the control of the droplet stream configuration and subsequent propagation. The technique has been shown to greatly reduce the intra-stream agglomeration over the conventional methods of perturbation, i.e., a sinusoidal disturbance, or a sinusoidal disturbance with an added harmonic. The new method of perturbation is considered a desirable feature of an LDR generator design by the present authors. The droplet production technique involves the use of an amplitude modulated sinusoidal waveform, and is discussed in detail in Ref 11. In brief, the fluid responds to the amplitude modulated disturbance by first breaking into droplets which are separated a distance corresponding to the wavelength of the fast frequency of the amplitude modulated disturbance. We call these droplets "carrier droplets." Unlike droplets generated with a conventional disturbance, each carrier droplet has associated with it a predictable relative speed. The relative speed is a direct consequence of the imposed amplitude modulated disturbance. Thus the disturbance essentially forces the carrier droplets in two adjacent half periods of the modulation to coalesce into a single drop. These "modulation" drops are measured to be much more stable than drops generated

with a pure sinusoidal disturbance. A physical explanation follows.

We consider all fluctuations of mass and momentum to arise at the break points of the fluid stream. If the break point is displaced, then one drop has an excess of momentum, and the neighboring drop has a deficit of the same amount of momentum. When the two drops coalesce, the fluctuations cancel, leaving the only sources of random fluctuations at the end points of the last two drops to merge. Thus the velocity dispersion, which is a measure of stream uniformity and is simply the ratio of the standard deviation of the unpredictable velocity fluctuations of the drops to the average drop speed, should decrease as 1/N, where N is the frequency ratio of the disturbance, or the number of carrier droplets that make up one modulation drop.

Figure 3 illustrates the results of applying an amplitude modulated disturbance to a single stream. The velocity dispersion at N=1 corresponds to the dispersion generated with a conventional waveform. The solid line represents 1/N.

Since the efficiency of the LDR depends on the high surface area to volume ratio of the drops, it is clear that the efficiency is maintained by suppressing unplanned droplet merging (see section 3.2). Thus, the new mode of perturbation is employed in the generator design. The effect of droplet speed dispersions on agglomeration is illustrated in Figure 4, (from Ref. 12) where it can be seen that for a typical flight distance of a LDR (50 m) a droplet speed dispersion of around 10^{-6} as required to prevent significant (10% of droplets) intra-stream agglomeration.

3.2 Multi-Stream Droplet Sheets

Consider the following example of a droplet radiator that is N_r droplet (or orifice) rows thick. The thickness of the sheet in numbers of radiation mean-free-paths is defined as

$$\Delta = \frac{\pi N_r}{4(\lambda_d/d)^2} \tag{1}$$

where λ_d is the nominal center to center spacing of droplets in a stream which in this case is also assumed to be the stream spacing in a row and d is the droplet diameter. The sheet's thickness in radiation mean-free-paths is useful to help characterize the efficiency of a droplet

sheet as a radiator; for $\Delta < 1$ the sheet emissivity varies approximately linearly with N_r or Δ. A simple calculation is informative. Say the Δ as defined above is set at 1. Assume streams of 100 μm droplets with a center to center separation of 3.5 diameters and thus $N_r \simeq 16$. Now, assume these agglomerate due to drop to drop speed differences within each stream. If on the average each drop combines with one other, the center to center distance has doubled and the drop diameter has increased by $2^{1/3}$, lowering Δ from 1 to 0.8 (note, since inter-stream spacing would not change, Δ changes only due to intra-stream droplet spacing and droplet diameters). Reducing Δ from 1 to 0.8 reduces the sheet emissivity by about 20%. If there is one further merging, Δ=0.65 which reduces the emissivity by 35%. Thus, modest amounts of agglomeration over a significant proportion of a sheet's area could have significant effects on the radiated power.

Similar comments about agglomeration also apply to inter-stream collisions caused by the angular dispersion of the nozzles, since for relative collision velocities less than about 2 m/s, 100 μm droplets tend to coalesce when they collide, at least for near head-on collisions. If we define three separate inter-droplet distances, λ_d the intra-stream separation, λ_{g1} the geometric separation of the nozzles in one row and λ_{g2} the separation between nozzle rows. The droplet number density is given by

$$n = \frac{1}{\lambda_d} \cdot \frac{1}{\lambda_{g1}} \cdot \frac{1}{\lambda_{g2}} \tag{2}$$

Assume a characteristic mean angular error of θ_c in the nozzle alignment. An approximate average relative speed of colliding droplets is $V_d \sin\theta_c$, where V_d is the speed of the droplets. The total collision cross-section is $\sigma_t = \pi d^2$ where d is the droplet diameter. There is some divergence due to the initial angular dispersion of the streams. Assume a droplet sheet initially w_o cm thick at the generator, thus there are $w_o/\lambda_{g2} = N_r$ rows of nozzles. At some point z from the generator the number of collisions one droplet experiences in a length dz is

$$N_c(z)ds = \frac{\sin\theta_c(\pi d^2)}{\lambda_d\lambda_{g1}\lambda_{g2}(1 + 2\sin\theta_c/N_r\lambda_{g2})}dz \tag{3}$$

Integrating, the total number of collisions for one droplet for a flight length L is

$$N_{ct} = \frac{\pi d^2 N_r}{2\lambda_d \lambda_{g1}} ln(\frac{2L \sin\theta_c}{N_r \lambda_{g2}} + 1) \quad (4)$$

For θ_c=2 mrad, L=50 m, N_r=10, d=100 μm, and $\lambda_d = \lambda_{g1} = \lambda_{g2}$=3.5d, the total number of collisions per droplet as the stream travels from the generator for 50 m is $N_{ct} = 5.3$. If the between-row spacing λ_{g2} is increased to 0.005 m (50d) N_{ct} =2, which relieves the inter-stream collision problem considerably, although not completely by any means. Note that if λ_{g1} is increased to 10d, which may be necessary to prevent the streams influencing each other due to wetting of the nozzle exit surface, the total number of collisions per droplet becomes N_{ct}=0.7.

There are all sorts of arguments about how much droplet agglomeration is acceptable. For the present design it was decided that the generator should provide a sheet with a small amount ($N_{ct} < 1$) of agglomeration. A relaxation of this requirement might be possible after careful system optimization studies.

4 DESIGN AND FLUID SELECTION

4.1 General Design Considerations

In order to identify fundamental problems associated with a flight capable design, the multi-stream generator is designed in a pre-prototype flight configuration. With obvious mass saving steps it could be suitable for use with a liquid droplet radiator. In this approach, any problems encountered with the operation of the generator provide practical design considerations for an actual flight module.

The most basic decision about the generator configuration has to do with the method that is selected to apply stream disturbances. Two possibilities have been examined. The first is the use of a fluctuating cavity pressure in the stagnation chamber for the streams ("cavity disturbance" mode). The fluctuating disturbance pressure that is superimposed on the stagnation pressure causes a periodic variation in mass flow in the streams which leads to a disturbance of the stream radii. The second possibility is to apply a disturbance directly to the nozzle array. The moving array may directly disturb the stream through viscous

effects at the nozzle walls. Also, the moving array can generate a fluctuating pressure in the stagnation cavity with the disturbance then being similar to the cavity disturbance mode. For reference purposes the moving nozzle case is distinguished by naming it the "orifice disturbance" mode.

Fluid lost due to partially blocked nozzles generating misdirected streams is a highly probable failure mode since small but continuous losses of fluid are fatal to the success of the LDR. The present generator design was accomplished keeping in mind conceptual design solutions for overcoming this problem. A pipe crawler for unplugging and/or plugging individual nozzles and a segment isolation scheme for cutting fluid flow to a limited number of nozzles using valves in the form of air bags or foam were hypothesized but not implemented. The generator design is compatible with the air bag or foam solutions since these were considered to be the simplest option. Additional particulate control to minimize nozzle plugging is incorporated with large areas of micron level filtering.

The parallelism of the nozzle array itself must be considered in the design to obtain the optimum stream spacing in order to prevent fluid loss or agglomeration. At present, the best orifice arrays that are easily obtainable can produce droplet streams with an angular standard deviation of several milliradians. It has been suggested (Ref. 13) that the parallelism of the nozzles in arrays may be improved with future studies.

All of the previous considerations must be integrated with the requirements of supplying a sufficient quantity of fluid with a minimum pressure drop over distances of typically 50 meters in a minimum mass device. In the design the assumption was made that fluid would be supplied at approximately working pressure; another option would be a high pressure supply system with local delivery by pressure regulators to the radiator modules. In the latter case our design would change somewhat, but not in any important way as far as the details of the stream generation are concerned.

4.2 Generator Design Details

The generator has been designed such that many modules may be connected in order to produce the desired number of streams for the Liquid Droplet Radiator. A conceptual

schematic of several connected generator modules is illustrated in Figure 5. To summarize the design configuration, micron filtered fluid reaches each orifice array through the fluid supply duct. The height of the duct is chosen so that the pressure drop over several connected modules is minimal (other considerations such as total fluid mass are important considerations which enter into the choice of the supply duct size but must be made by optimizing the entire LDR system). A filter plate with a pore size of 2-3 μm separates the fluid stagnation chamber from the fluid supply duct. In the event of misdirected streams, the actual flight model can employ the segment isolation scheme by inflating an air bag or injecting foam into the stagnation chamber of a module. The generator design is capable of holding five orifice arrays which are each 0.13 m in length. Each orifice is 100 microns in diameter so that for a 5 diameter stream spacing with end clearances a single array contains 1250 orifices. For preliminary testing a single array 0.066 m in length was used with orifice separations of 5 and 10 nozzle diameters. For final testing, a 0.13 m array with 100 orifices was studied.

We have examined two methods of applying an amplitude modulated disturbance to initiate the radial instability of the stream. The first method considered is to form a disturbance in the stagnation cavity by inserting an isolated piezoelectric crystal under the filter plate. In this case, it is desirable to isolate the crystal from the structure in order to inhibit any unwanted structural vibrations. The crystal must also be shielded from the fluid since the fluid in the liquid droplet radiator will be sufficiently hot to exceed the Curie point of the crystal. To attain a velocity dispersion around 10^{-6} it has been found that pressure fluctuations (in the form of an amplitude modulated waveform with a high frequency ratio) of several percent of the stagnation pressure are required for 40 cSt fluid[10]. To reach these levels while using the cavity disturbance mode of operation requires using a crystal that is large compared to the separation between the crystal and the orifice or to operate at conditions corresponding to a cavity resonance. The second mode of stream perturbation relies on nozzle motion. In this case, the piezoelectric crystal is mounted on the exit face of the orifice array. It is necessary to design the oscillating orifice assembly such that excessive vibrations are not introduced into the structure. An advantage associated with orifice disturbance mode is that it is easier to have the fluid cavity only about 0.01 m high while still supplying sufficient

fluid to the orifice array. Also, the crystal does not come in direct contact with hot fluids. In this mode of operation the stream disturbance originates from the pressure field at the surface of the vibrating orifice array and from the direct influence of mechanical motion of the orifice.

Both methods of perturbation application have been tested and yield similar results. Figures 6 and 7 illustrate the results of the uniformity of single streams of fluid when perturbed with the cavity disturbance mode (Figure 6) and the orifice disturbance mode (Figure 7) for streams of $1x10^{-5}$ m^2/s (10 cSt) DC-200 fluid. Figures 6 and 7 were obtained with a conventional sinusoidal disturbance applied to the fluid stream. Since the two modes of operation give similar results, and due to the advantages described, the orifice disturbance mode of operation has been incorporated into the generator design. Figure 8 illustrates an enlarged cross-section of the generator module showing the piezoelectric crystal and nozzle arrangement chosen.

The orifices have been formed directly in the oscillating assembly shown in detail in Figure 9. For operation, the piezoelectric crystal is bonded onto the exit face of the orifice array. The crystal and array configuration are placed onto a ceramic insulating seat. Power is provided to the crystal through a wire which feeds through the ceramic and onto a brass washer which lies between the ceramic insulator and the piezoelectric crystal. The assembly was designed such that the angular deflection due to bending of the orifice array when subjected to a load of $1.034x10^6$ Pa (150 psi) is less than 5 μrad. The angular twist of the array, which may result if the surface of the crystal and the surface of the ceramic insulating seat are not parallel, was calculated to be significantly less than one 1 mrad. Careful attempts have been made to make the joining parts parallel.

4.3 Fluid Selection

Performance testing of the multi-stream generator was required with the use of two different fluids having viscosities of $1x10^{-5}$ and $4x10^{-5}$ m^2/s (10 and 40 cSt). Original plans called for the use of DC-200 at the $1x10^{-5}$ (10 cSt) viscosity, and DC-704 at $4x10^{-5}$ (40 cSt). Both fluids are silicone based low vapor pressure diffusion pump oils. DC-200 has the

convenience of being available in a variety of viscosities, and it is considerably less expensive than DC-704. However, the use of two fluids with as wide a variety in surface tension as possible was desirable. The surface tension of DC-704 is about twice that of DC-200, thus the two aforementioned fluids were chosen for use with the generator.

After testing the generator with the $1x10^{-5}$ (10 cSt) DC-200, and switching to the DC-704, several practical problems were encountered. The most significant was that the two fluids do not mix with each other. We found the DC-704 contained a suspension of the residual traces of DC-200 left in the system. The resulting fluid appeared to have a nonuniform surface tension, and furthermore, data taken with the mixture was not representative and is not included in this report. It was necessary to clean the apparatus thoroughly of the fluid mixture. This was done by dismantling as much of the system as possible followed by kerosene and alcohol purges. For subsequent tests DC-200, at the $4x10^{-5}$ (40 cSt) viscosity was used in lieu of the DC-704. The surface tension is not expected to have a significant effect since the growth factor varies as $(\sigma/\rho_o)^{1/2}$, where σ is the surface tension. The density of all these fluids is around 10^3 kg/m^3 so that there is not a big difference in $(\sigma/\rho_o)^{1/2}$ for a factor of two difference in σ.

5 GENERATOR FABRICATION

Drawings of the generator design were submitted to NASA and approved for fabrication. The majority of the generator was fabricated in the USC School of Engineering's machine shop. Two different orifice arrays were made for reasons which are discusssed in Section 6. One was fabricated by Du Pont Precision and has 100 orifices, each 100 μm in diameter by 300 μm long. It was produced from hardenable stainless steel. The orifices were measured by Du Pont to be accurate in diameter and roundness to ± 2 μm. Perpendicularity of the orifices to the lapped reference plane was nominally specified to better than ± 2 mrad during the manufacturing process. The orifices were also nominally specified to be parallel to each other to better than ± 3 mrad. The second array, which was drilled in aluminum by NASA Lewis has 4, 100 μm diameter orifices. As shown in Figure 9, array plates are bonded directly to a piezoelectric crystal which has the shape of a "race-track." The array and crystal assembly

rest on top of a brass washer, and the entire assembly fits in a ceramic insulating seat. Both the ceramic seat and the "race-track" shaped piezoelectric crystal were machined by Duramic Products Inc. and Mindrum Precision respectively. Electrical contact is made to the piezoelectric crystal by a wire which feeds through the ceramic seat and makes contact with the brass washer.

6 TESTING

The contract required an investigation of the operation of the droplet generator with a 0.13 m long, 100 hole array. Test conditions included the use of two different droplet fluids of different viscosity and three different stream speeds.

Two preliminary arrays were tested prior to the machining of the final 0.13 m array in order to uncover any problems. Each array assembly was configured as shown in Figure 9. One array was drilled by NASA Lewis, and contains 53 holes with 10 diameter spacing between holes. The array was machined out of aluminum. The second array was machined out of stainless steel and was fabricated by Du Pont Precision with the same tolerances as described above. It contains 109 holes with 5 diameter spacing between holes. Each array is 0.05598 m (2.20 inches) long and the orifices are 100 μm in diameter. The preliminary tests showed that the array which was fabricated by Du Pont produced droplet streams which were significantly more parallel than the array drilled by NASA Lewis. However, the angular dispersion was great enough with the Du Pont array to prohibit the ready identification of particular streams after they had traveled 5.5 m. For this reason, two 0.13 m arrays were manufactured for the final testing phase. The first was fabricated by Du Pont Precision and contained 100 holes, each 100 μm in diameter. This array was used for testing the overall generator performance and the angular dispersion of the array. The second array which was drilled by NASA Lewis contained 4 holes and was used for measuring the velocity dispersions of the individual streams as a function of disturbance wavenumber. The electric power consumed by the array oscillating in the droplet generator was measured. The several measurements will be discussed in more detail in Sections 6.2 through 6.4.

6.1 Experimental Apparatus: Droplet Dynamics Space Simulator

The facility in which the droplet streams are generated, measured and observed is the Droplet Dynamics Space Simulator, shown in Figure 10. The apparatus is an isolated body, suspended from its center of gravity by four vibration isolation mounts which filter motion above frequencies of 1 Hz. The main component is a vertically suspended optical bench on which a 5.5m long; 0.25m diameter stainless steel flight tube, two diffusion pumps, sensors and optics are mounted. Optical access is provided to the tube at its top and bottom ends. Recycled, out-gassed fluid is supplied to the multi-stream droplet array mounted at the top of the flight tube. A flexible rubber diaphragm is used to separate the high pressure gas (which drives the flow) from the droplet fluid. This is necessary since high pressure gas dissolves in the fluid, leading to cavitation when the fluid is ejected into a vacuum.

The piezoelectric crystal which initiates the stream instability is driven by two phase-locked function generators that are controlled by a high-stability reference source. The function generators are used to provide a stable, amplitude-modulated signal. For a conventional constant amplitude sinusoidal signal, only one generator is needed.

The detector used to image the droplet streams at the lower observation port is illustrated in Figure 11. The image of the droplet stream is superimposed onto the receiving slit of the detector. The detector essentially consists of a receiving slit which is positioned perpendicular to the image of the droplet stream, and just in front of a photomultiplier tube. The shadow image is then passed through a cylindrical lens in order to illuminate a large portion of the photomultiplier tube's photocathode. Careful attempts were made in the design of the detector in order to capture an accurate representation of the droplet stream profile. The design characteristics of the detector are discussed in detail in Ref. 12.

A schematic of operation is sketched in Figure 12. To measure the uniformity of the droplet stream, a light beam is split and sent through the optical access ports. The beam is sent through a spatial filter in order to filter out any optical noise due to particulates entering the light field. As the droplet stream passes through the light, its magnified shadow image is reflected onto the receiving slit of the detector. Each droplet image that passes over the slit causes a dip in the light flux received by the slit. The corresponding signal consists

of a series of dips representing droplets. The output signal from the photomultiplier tube is digitized and recorded with a waveform recorder at selectable rates up to 20 MHz, and the resulting digital codes are stored in up to 16k words of memory. Once stored in memory, the recorded droplet stream waveform is output in both digital and analog formats and stored for later evaluations and measurements by computer. Typically, waveforms consisting of up to 400 droplets were captured and analyzed.

6.2 Overall Generator Performance

The overall generator performance was measured with the use of still photography. Preliminary tests were made with two small orifice arrays as discussed previously. One array had 53 holes with a 10 droplet diameter spacing, and the other had 109 holes spaced 5 droplet diameters apart. No significant differences were found in the performance of the two arrays, or interactions between the streams due to surface wetting. Final testing was done with two 0.13 m arrays; one with 100 holes which was fabricated by Du Pont Precision, and one with four holes used for velocity dispersion measurements which was drilled by NASA Lewis. Figure 13 is a photograph of the 0.13 m, 100 hole array in operation. In this particular photograph, the droplet fluid is DC-200 at 4×10^{-5} m^2/s (40 cSt), and the stream's speed was 40 m/s. Similar photographs were taken for the other conditions. The specifics of the angular dispersion and the velocity dispersions of the streams will be discussed in the following sections.

6.3 Angular Dispersions

The angular dispersion of the 100 hole array was measured with the following method. First, a laser sheet was created which was several centimeters wide, several millimeters thick and spanned the horizontal distance of the observation chamber. By allowing the droplet streams to travel through the laser sheet in an approximately perpendicular direction, and by photographing the resulting forward scattering, we have been able to determine the angular spread of the array of streams. For data reduction, a photograph was taken of a grid which was placed in the chamber at the same orientation as the laser sheet. Deviations of the

stream's displacements from the centerline of the array were measured by superimposing the images of the scattered light patterns from the streams and the grid. A standard deviation of the angular spread was found by measuring the deviation of each stream from the centerline, forming an average displacement and calculating the standard deviation. Table 1 gives the results of the angular dispersion measurements at the indicated conditions. All measurements are in mrad. The result indicated with an asterisk is an estimated standard deviation, for in this case trouble was encountered separating the images of the scattered light due to overexposed film. Note that the angular dispersion that was calculated is for the direction perpendicular to the line of orifices. The higher dispersion observed for the 10 cSt fluid has no obvious explanation. Generally it is observed that angular dispersions are sensitive to dissolved gas in the liquid. The 10 cSt experiments were the initial experiments in this study. It is possible that because they also involved a first use of a new high capacity oil recirculation system, some dissolved gas may have been present in these experiments.

Table I Angular Dispersions Perpendicular to Orifice Row (mrad) for a 109 Stream Array

	DC-200, 10cSt	DC-200, 40cSt
10 m/s	18.1	8.8
20 m/s	16.9	8.8
30 m/s	11.5*	8.9

6.4 Velocity Dispersions

Both arrays were studied to measure velocity dispersions using both fluids. The uniformity of a single stream from the 109 hole array with the $1x10^{-5}$ m^2/s (10 cSt) fluid was measured and it was found that the stream had a velocity dispersion of $1.25x10^{-6}$ when perturbed with an amplitude modulated waveform with a frequency ratio of 4:1. A trace of this droplet waveform is illustrated in Figure 14. Following this experiment, the NASA four hole array was tested (Figure 15). It was only possible to analyze the performance of three of the streams, as the fourth orifice was misdirected at an extreme angle, and the apparatus

could not be maneuvered enough to locate it. Figures 16, 17, and 18 illustrate the array performance, where orifices #1, #2, and #3 are in consecutive order as they appear on the array. It can be seen that all orifices tested respond generally in the same way. For these results, the streams were perturbed with an amplitude modulated waveform with a frequency ratio of 4:1. When the streams were perturbed with a conventional sinusoidal waveform they were observed to be less uniform. Only the data points generated with an amplitude modulated waveform with a frequency ratio of 4:1 were saved and are included in Figures 16 through 18. From the figures it can be seen that the velocity dispersions are as high as $1x10^{-4}$. The measurements are not as low as the measurement obtained with the Du Pont array. This finding was investigated in a preliminary way and it appears that the difference in uniformity was due to a difference in the perturbation amplitude which was applied to the stream. When the NASA Lewis array was tested, the power amplifier was unserviceable. Unfortunately, use had to be made of an amplifier which outputs $\sim$ 10 V. The amplifier that was used to test the Du Pont array typically outputs $\sim$ 70 V. In retrospect, it appears that the disturbance amplitude was in a region where higher voltage to the piezoelectric crystal is necessary for obtaining ultra-coherent streams of drops (with velocity dispersions near $1x10^{-6}$) from the array, when using the orifice disturbance mode of operation along with an amplitude modulated disturbance at large frequency ratios. We are currently studying the effects of absolute amplitude of the driving perturbations on the velocity dispersion of the breakup of a single stream of drops. At this stage in the investigation, it appears that the amplitude plays a significant role in the velocity dispersion of the drops for the range of disturbance amplitude that was employed in the tests described previously.

Following the work with the $1x10^{-5}$ m^2/s (10 cSt) fluid, a switch was made to the $4x10^{-5}$ m^2/s (40 cSt) fluid. DC-200 was used in both cases as discussed in Section 4.3. For this work, the amplifier which output $\sim$ 70 V was available for all measurements. Measurements with both the Du Pont array and the NASA Lewis array were similar. Figures 19, 20, and 21 illustrate the NASA array performance with the $4x10^{-5}$ m^2/s (40 cSt) fluid. For each data point, the streams were perturbed with an amplitude modulated disturbance with a frequency ratio of 4:1. For reasons that are not known it was only possible to test the

array at 20 m/s and at 30 m/s when using the $4x10^{-5}$ m^2/s (40 cSt) fluid. The 10 m/s stream's velocity dispersion was very high, which was unexpected. It can be seen that the velocity dispersions for the 20 and 30 m/s are for the most part near a few times 10^{-5}, which by the current standards at USC (when using an amplitude modulated disturbance at large frequency ratios) are considered to be about an order of magnitude high. One plausible explanation for these results is that the orifice disturbance mode of operation had not previously been tested with a highly viscous fluid. In other studies at USC, highly viscous fluids were tested only while using the cavity disturbance mode. It is believed that the cavity disturbance mode as it was used in that work provided a greater amplitude disturbance than the orifice disturbance mode. A greater disturbance amplitude may be necessary to breakup the more viscous fluids into droplet streams with very low velocity dispersion (see following section on acoustic analysis and resulting design implications).

6.5 Power Measurement

Power measurements were made for typical generator operating conditions of 100 psi, and 50kHz carrier frequency, 40 cSt fluid and the 0.13 m long orifice array. The measurements were obtained by observing voltage drops using a differential plug-in amplifier for an oscilloscope and a 6Ω resistor in the supply line to the piezoelectric crystal. The resistor was about 0.5 m from the crystal. The supply line was loaded with a $10^4\Omega$ shunt to ground between the 6Ω resistor and the power supply. Simultaneous measurements using a dual beam oscilloscope were made of the applied voltage and the current passing through the 6 Ω resistor. It was observed at 50 kHz that the voltage and current were in- phase and corresponded to an average power consumption of 6.5 watts. This compares to an average current flow of about 0.05 amps required to charge the capacitor (the RC time constant of the 6Ω piezoelectric circuit is less that 10^{-7}s). The power required to move a piston against 100 psi from the minimum to maximum deflection of the crystal (about 0.2 μm) 50×10^3 times a second is around 8 watts, assuming that the energy injected into the fluid is completely dissipated.

6.6 Satellites

For streams disturbed with an amplitude modulated disturbance the existence of satellites is not expected after the streams have coalesced to modulation drops. For the measurements done in this study no satellites were observed.

7 ACOUSTIC ANALYSIS

In order to help understand the mechanisms by which a disturbance is applied to the droplet stream from the generator, both theoretical and experimental studies have been completed. The theoretical work is detailed in Section 7.1 and the experiments in Section 7.2.

Table 2

Parameter Values Used in the Acoustic Analysis

Parameter	Typical Value
L_x	0.10 m
L_y	0.10 m
L_z	0.02 m
ℓ_x	0.01 m
ℓ_y	0.01 m
ε	0.1×10^{-6}m
ρ_o	100 kg/m^3
c	3000 m/s
ν	4.16×10^{-5} m^2/s
ω	$< 300 \times 10^3$Hz

7.1 Theory

Consider a rectangular cavity with characteristic dimension L_x, L_y, L_z subjected to external forcing by means of a rectangular piston with side lengths ℓ_x, ℓ_y. The geometrical

configuration is sketched in Figure 22. The parameters ε and ω denote the amplitude and circular frequency of the excitation, respectively. The medium is assumed to be homogeneous and at rest, of density ρ_o and speed of sound c. Kinematic viscosity is ν, dilatational viscosity is η. Typical values of interest for all these parameters are listed in Table 2. The main purpose of the present calculation is to obtain the value of the perturbation pressure at the center of the piston as a function of forcing frequency and of the other parameters in the problem.

7.1.1 Preliminary Assumptions: Effects of Viscosity

According to classical results [14,15,16] a plane wave $e^{i(kx-\omega t)}$ moving in a duct of cross-sectional length scale L filled with a viscous and heat-conducting fluid, is characterized by the following complex wavenumber k

$$k \approx \frac{\omega}{c} + \frac{1+i}{\sqrt{2}}\left(1 + \frac{\gamma-1}{\sqrt{Pr}}\right)\frac{(\nu\omega)^{1/2}}{cL} + \frac{i}{2}\left(\frac{\gamma-1}{Pr} + \frac{\eta}{\rho_o\nu}\right)\frac{\nu\omega^2}{c^3}, \tag{5}$$

where γ is the ratio of specific heats and Pr the Prandtl number. In this expression, the first term is the classical propagation term of inviscid sound waves in an unbounded medium. The second term represents attenuation and dispersion effects due to the presence of viscous Stokes layers (unsteady perturbation boundary layers) at the walls of the tube. The thickness of these layers is of order $\delta \sim [(2\nu)/\omega]^{1/2}$. Finally, the third terms accounts for dilatational attenuation of acoustic waves in the bulk of the fluid. We shall assume that the excitation frequency is such that the hierarchy of these various terms is respected, namely

$$\frac{(\nu\omega)^{1/2}}{cL} \ll \frac{\omega}{c} \quad and \quad \frac{\nu\omega^2}{c^3} \ll \frac{(\nu\omega)^{1/2}}{cL} \tag{6a, b}$$

Under these conditions, dissipation effects can be neglected altogether. Thus the range of frequencies of interest is restricted to be

$$\frac{\nu}{L^2} \ll \omega \ll \left(\frac{c^4}{\nu L^2}\right)^{1/3} \tag{7}$$

The first inequality states that viscous dissipation in the Stokes layers is negligible whereas the second inequality states that bulk dissipation is negligible compared to Stokes layer

dissipation. For the values listed in Table I, it is therefore legitimate to neglect at leading order viscous damping, provided the excitation frequencies are chosen within the range

$$4 \cdot 10^{-3} \ll \omega \ll 10^{6}$$

These conditions appear to be satisfied in practice and we shall neglect viscous dissipation effects.

7.1.2 Mathematical Model:

The governing equations of linear sound propagation in a fluid medium at rest are given by

$$\frac{\partial \rho}{\partial t} + \rho_o \nabla \cdot \vec{V} = 0 \tag{8}$$

$$\rho_o \frac{\partial \vec{V}}{\partial t} = -\nabla p \tag{9}$$

$$p = c^2 \rho \tag{10}$$

where ρ, p and $\vec{V}$ denote the perturbation density, pressure and velocity, respectively. The boundary conditions are

$$\vec{V} \cdot \vec{n} = 0 \text{ on all walls except piston,} \tag{11a}$$

$$w = \frac{\partial Z_p}{\partial t} = -i\omega\varepsilon e^{-i\omega t} \ \ on \ \ Z = -\frac{L_z}{2}, \mid x \mid < \frac{\ell_x}{2}, \mid y \mid < \frac{\ell_y}{2}. \tag{11b}$$

In the above, the piston displacement $Z_p = \varepsilon e^{-i\omega t}$ and $\vec{n}$ is the unit normal. The Z-component of the perturbation velocity is denoted by w.

It is convenient to reformulate the entire problem in terms of perturbation pressure only. One readily obtains the following system:

$$\frac{\partial^2 p}{\partial t^2} - c^2 \nabla^2 p = 0 \tag{12}$$

$$\nabla_p \cdot \vec{n} = 0 \text{ on all walls except piston} \tag{13a}$$

$$\frac{\partial p}{\partial z} = \rho_o \varepsilon \omega^2 e^{-i\omega t} \tag{13b}$$

on

$$z = -\frac{L_z}{2}, \mid x \mid < \frac{\ell_x}{2}, \mid y \mid < \frac{\ell_y}{2}$$

7.1.3 Normal Modes of Rectangular Cavity

The natural modes of the cavity can be sought in the absence of external excitations. We look for solutions of the form

$$p = \psi(x, y, z) e^{-i\omega t} \tag{14}$$

After substitution into the previous system, one obtains the eigenvalue problem

$$\nabla^2 \psi + k^2 \psi = 0 \tag{15a}$$

$$\nabla \psi \cdot \vec{n} = 0 \text{ on all walls,} \tag{15b}$$

where $k = \omega / c$ is the unknown eigenvalue

Resonances can be determined by a straightforward separation-of-variable analysis. The eigenfunctions are found to be

$$\psi_{n_x, n_y, n_z}(x, y, z) = \cos(\frac{\pi n_x}{L_x} x + \frac{\pi n_x}{2}) \cos(\frac{\pi n_y}{L_y} y + \frac{\pi n_y}{2}) \cos(\frac{\pi n_z}{L_z} z + \frac{\pi n_z}{2}) \tag{16}$$

and the corresponding eigenvalues, or resonance frequencies, are given by

$$k^2_{n_x, n_y, n_z} \equiv (\frac{\omega_{n_x, n_y, n_z}}{c})^2 = (\frac{\pi n_x}{L_x})^2 + (\frac{\pi n_y}{L_y})^2 + (\frac{\pi n_z}{L_z})^2 \tag{17}$$

The indices n_x, n_y, n_z may take all zero or positive integer values. The eigenfunctions are endowed with the following orthogonality properties:

$$\int_v \psi_n \psi_m dV = V \Lambda_n \delta_{mn} \tag{18}$$

For simplicity we have denoted by n or m distinct triads (n_x, n_y, n_z). The symbol δ_{mn} is the Kronecker delta

$$\delta_{mn} = \begin{cases} 1 & m = n \\ 0 & m \neq n \end{cases} \tag{19}$$

and the quantity Λ_n is such that

$$\Lambda_n = \frac{1}{\varepsilon_{nx}\varepsilon_{ny}\varepsilon_{nz}} \qquad\qquad \varepsilon_{nx} = \begin{cases} 1 & n_x = 0 \\ 2 & n_x > 0 \end{cases} \tag{20}$$

The quantity V is the cavity volume $V = L_x L_y L_z$.

7.1.4 Green's Function of Rectangular Cavity:

For future use, it is necessary to obtain the impulse response (or Green's function) of the cavity when it is subjected to a delta-function excitation of frequency ω at an arbitrary location $\vec{r}_o$. The mathematical problem of interest is then

$$\nabla^2 G_\omega + k^2 G_\omega = \delta(\vec{r} - \vec{r}_o) \tag{21}$$

$$\nabla G \cdot \vec{n} = 0 \text{ on all walls}$$

Upon assuming an expansion of G_ω in the previous eigenfunctions, one generates the solution

$$G_\omega(\vec{r} \mid \vec{r}_o) = \sum_n \frac{\psi_n(\vec{r}_o)\psi_n(\vec{r})}{\Lambda_n V[(\omega/c^2 - k_n^2]} \tag{22}$$

As before, triads (n_x, n_y, n_z) are given the collective name n. Note that the above impulse response blows up at the resonant frequencies $\omega_n = ck_n$, as expected.

7.1.5 Forced Response Due to Piston Motion:

One may now tackle the original problem at hand specified by equations (12)-(13). Steady-state solutions are sought in the form

$$p(x,y,z,t) = p_\omega(x,y,z)e^{-i\omega t} \tag{23}$$

where ω is the excitation frequency specified in (9b). The unknown p_ω satisfies

$$\nabla^2 p_\omega + k^2 p_\omega = 0 \tag{24}$$

$$\nabla p_\omega \cdot \vec{n} = 0 \text{ on all walls except piston surface} \tag{25a}$$

$$\frac{\partial p_\omega}{\partial n} = \nabla p_\omega \cdot \vec{n} = \rho_o \varepsilon \omega^2 \text{ on piston surface S at } z = -L_z/2 \tag{25b}$$

A straightforward application of Green's theorem allows us to relate the values of the pressure gradient at the piston surface to the pressure field p_ω within the cavity. One obtains the solution

$$p_\omega(\vec{r}) = -\int_S G_\omega(\vec{r} \mid \vec{r}_o)\frac{\partial p_\omega}{\partial n}(\vec{r}_o)dS(\vec{r}_o) \tag{26}$$

Thus the pressure field within V is seen to be due to a distribution of point sources of strength

$$\frac{\partial p_\omega}{\partial n}(\vec{r}_o)dS(\vec{r}_o)$$

located on the piston surface S. The total pressure field is simply obtained by superposition of all the corresponding impulse responses, as stated in (26). The pressure gradient on S is known from (25b) and the Green's function G_ω has been calculated [see equation (22)] previously for an arbitrary source location $\vec{r}_o$. After some calculations, one generates the pressure field within the cavity:

$$p_\omega(\vec{r}) = \frac{\rho_o \varepsilon \omega^2}{\pi^2 L_z} \sum_{m,n,p \geq 0} \frac{\sin(\pi m \ell_x / L_x) \sin(\pi n \ell_y / L_y)}{mn[k_{m,n,p}^2 - (\omega/c)^2]\Lambda_{mnp}}$$

$$\cdot \cos(\frac{2\pi m x}{L_x}) \cos(\frac{2\pi n y}{L_y}) \cos[\frac{\pi p}{L_z}(z + \frac{L_z}{2})] \tag{27}$$

with

$$(\frac{\omega_{m,n,p}}{c})^2 = k_{m,n,p}^2 = (\frac{2\pi m}{L_x})^2 + (\frac{\pi n^2}{L_y} + (\frac{\pi p}{L_z})^2 \tag{28}$$

and

$$\Lambda_{mnp} = \frac{1}{\varepsilon_m \varepsilon_n \varepsilon_p} \varepsilon_i = \begin{cases} 1 & i = 0 \\ 2 & i \neq 0 \end{cases} \tag{29}$$

As expected, the response blows up if the excitation frequency ω coincides with one of the resonant frequencies $\omega_{m,n,p}$.

In the low frequency limit $\omega \to 0$, the general formula (27) simplifies considerably:

$$p_\omega(\vec{r}) \approx -\frac{\rho_o \varepsilon \ell_x \ell_y c^2}{L_x L_y L_z} + 0(\omega^2), \omega \to 0. \tag{30}$$

this relation provides a simple scaling relation at excitation frequencies which are far from resonance frequencies. It is worth noticing that, in the low frequency limit, the pressure is uniform within the cavity, at leading order.

The pressure p_ω at the center of the piston is given by

$$p_\omega(0, 0, \frac{L_z}{2}) = \frac{\rho_o \varepsilon \omega^2}{\pi^2 L_z} \sum_{m,n,p \geq 0} \frac{\sin(\pi m \ell_x / L_x) \sin(\pi n \ell_y / L_y)}{\Lambda_{mnp} mn[k_{m,n,p}^2 - (\omega/c)^2]} \tag{31}$$

7.2 Results Based on Acoustic Analysis and Some Experiments

Programs have been written to display graphically the response curve $p_\omega(0, 0, L_z/2)$ given by (31) as a function of excitation circular frequency ω. Typical results are shown in Figures 23 and 24. The first few resonances appear to intrude into the frequency range of interest, as seen from Figure 23 where one detects the pervading influence $\omega_{0,1,0}$ (or $\omega_{1,0,0}$) and of

$\omega_{1,1,0}$. Figure 24 shows the pressure response in the lower part of the spectrum below the 1st resonance frequency. The exact location of the resonances is likely to be sensitive to the shape of the cavity. The order of magnitude of p_ω outside the resonance regions is likely to be fairly insensitive to the particular shape of the cavity.

As a check on the validity of the analysis we observed pressures in the stagnation chamber using the cavity disturbance technique. The cavity is illustrated in Figure 2 of Ref. 11. The predicted cavity pressures as a function of frequency are shown in Figure 25 along with several measured pressures. The "cavity" was cylindrical in shape so that the predictions are only expected to be approximate. The piston is a piezoelectric crystal forming one end of the cavity (see Figure 2, Ref. 11). The data points are the measured amplitudes of the pressure fluctuations in the cavity. Note that the predictions and measurements are in order of magnitude agreement.

Predictions were made for the multi-stream generator and are shown in Figure 26. For this case because the area of the moving orifice array (see Figure 9) is relatively smaller than in the cavity disturbance mode experiments, the low frequency pressures are smaller (see Eqn. 30). Also, due to the configuration of the orifice assembly, significant structural vibrations were transmitted and observed, making it impossible to measure cavity pressures with our piezoelectric pressure transducer in the multi-stream droplet generator. Relying on the prediction it is apparent that in future designs, using the orifice disturbance mode of operation, it would be useful to have individual stagnation cavities for each orifice array, such that the moving array and its mount form the complete surface area of the bottom of each cavity. Such an arrangement will result in maximum pressure being achieved in each stagnation cavity. For the present design, simply walling off each moving array would increase the pressures and change its frequencies, as shown in Figure 27.

8 LARGE SCALE GENERATOR DESIGN

As part of the contract a preliminary design of a nominal 5000 orifice generator segment was required. The large scale generator designs are shown in Figures 29 through 33. The design is similar to the laboratory generator fabricated for this contract. The orifice distur-

bance mode of perturbation was employed in the design because of the advantages described in section 4.2. It is believed that any shortcomings found in the results due to the amplitude limitations of this mode of motion can be overcome by decreasing the stagnation cavity volume as described in the previous section.

The proposed nominal 5000 stream generator segment incorporates walls associated with the bottom plate of the generator (see Figure 31). The walls not only serve to reduce the volume of the stagnation cavities but act to increase significantly the moment of inertia of the bottom plate, thus making the design more efficient from a structural perspective. Additionally, divider walls can be added at periodic intervals as illustrated in Figure 31, which changes the resonance characteristics and also increases the structural integrity of the bottom plate. The resulting pressure predictions are shown in Figure 28. Note the disappearance of the resonant peaks at the lowest frequency. More work needs to be done, however, to determine accurately the amplitudes required for highly uniform drops as a function of fluid viscosity.

A schematic of the nominal 5000-orifice droplet generator is illustrated in Figure 29. This particular schematic shows a cut-away of the generator, exposing the fluid supply duct, filter plate and array assembly. The generator is 0.616 m (24.25 inches) long, and contains 20 arrays. Figure 30 shows a further cut-away illustrating the generator's configuration. Figure 31 shows a top view and a side view of the array holder. The assembly was designed such that the angular deflection due to bending of the orifice array when subjected to a load of 150 psi is less than 5 μrad. Figure 32 shows a side view of the assembled generator. Lastly, Figure 33 illustrates the orifice array assembly. Each of the 20 arrays can contain in a single row 260 orifices which are 100 μm in diameter, at 5 diameter spacings. The mass of the generator illustrated in Figure 29 and 31 is about 1.2 gms per orifice (5200 orifices) using aluminum for the structural components. For carbon fiber composite structural components the mass is around 0.9 gms per orifice.

9 SUMMARY OF RESULTS

A multi-stream laboratory generator was designed and fabricated in a pre-prototype configuration which would be potentially suitable for use with a Liquid Droplet Radiator. The generator was tested using two orifice arrays; one drilled by NASA Lewis, and the other fabricated by Du Pont Precision. Two fluids with viscosities of $1x10^{-5}$ m^2/s (10 cSt) and $4x10^{-5}$ m^2/s (40 cSt) were also used. Stream speeds were 10, 20, and 30 m/s. Angular dispersions of the streams from the 100 orifice Du Pont array were measured and no significant variation with stream velocity was found. The $4x10^{-5}$ m^2/s (40 cSt) fluid appears, at around $\pm 9\mu$rad, to have smaller angular dispersion than the $1x10^{-5}$ m^2/s (10 cSt) fluid. However, the resolution obtained when photographing the $4x10^{-5}$ m^2/s (40 cSt) streams was much greater than the resolution obtained when photographing the $1x10^{-5}$ m^2/s (10 cSt) streams and in retrospect there was a possibility of dissolved gases in the fluid during the 10 cSt experiments. Velocity dispersions were also measured. It was discovered that in the parameter range that was investigated, the amplitude of the disturbance applied to the stagnation cavity is an important parameter in obtaining ultra-coherent streams of droplets. It is also presumed that the more viscous fluid requires a higher power to the crystal (larger crystal deflection) than does the lower viscosity fluid, although this presumption must be verified in future investigations. The velocity dispersions for streams from several positions along the 0.13 m orifice array were similar.

A conceptual design for a 5200 stream generator was completed, incorporating ways to generate higher disturbance amplitudes than was possible in the laboratory generator. Otherwise the design is similar to that of the laboratory generator.

APPENDIX I: NOMENCLATURE

c speed of sound

d droplet diameter

d_o orifice a nozzle diameter

$G_\omega(\vec{r} \mid \vec{r}_o)$ Green's functions

k non-dimensional wavenumber for acoustical analysis

k_o non-dimensional wavenumber for a capillary streams $((\lambda/\pi d_o)^{-1})$

$\ell_{x,y}$ dimensions of surface containing the orifice array

L droplet flight length or characteristic dimensions in acoustic analysis

$L_{x,y,z}$ dimensions of stagnation cavity

n droplet number density

$\vec{n}$ unit normal vector

N frequency ratio of amplitude modulated waveform

N_{ct} total number of collisions one droplet experiences

N_r number of rows of droplet streams

p perturbation pressure

P_r Prandtl number

$\vec{r}_o$ source position vector

t time

V stagnation cavity volume

$\vec{V}$ perturbation velocity

V_d speed of droplets

w_o thickness of droplet sheet at generator

β amplitude growth factor

γ ratio of specific heats

Δ thickness of sheet in radiation mean free paths

ϵ amplitude of orifice array displacement

η dilatational viscosity

θ_c angular error of stream alignment

λ center to center spacing of drops, also disturbance wavelength of carrier waveform

λ_d intra-stream separation

λ_{g1} geometric spacing of nozzles

λ_{g2} separation between rows

λ_ω wavelength of disturbance imposed as a capillary stream

Λ quantity in acoustic analysis

ν kinematic viscosity

ρ perturbation density

ρ_o density of liquid in stagnation cavity

σ surface tension

σ_t collision cross-section of droplet

ψ_{n_x,n_y,n_z} eigenfunction

ω circular frequency

References

[1]A.T. Mattick and A. Hertzberg. "The Liquid Droplet Radiator — an Ultralightweight Heat Rejection System for Effective Energy Conversion in Space", Acta Astronautica 9, pp165-172, 1982

[2]K.A. White. "Liquid Droplet Radiator Status," AIAA preprint 87-1537, June 1987

[3]M.T. Plateau. "The Theory of Sound," edited by Lord Rayleigh, Vol II, New York, p360, 1945

[4]F. Savart. "Memoire sur la Constitution des Veins Liquides Lancees par des Orifices Circulaires en Mince Paroi," Annles de Chimie, 53, pp337-386, 1833

[5]Lord Rayleigh. "On the Instability of Liquid Jets," Proc. R. Soc. Lond., A29, p71, 1878

[6]M.C. Yuen. "Non-linear Capillary Instability of a Liquid Jet," J. Fluid Mech., 33, Part 1, pp151-163, 1968

[7]A.H. Nayfeh. "Nonlinear Stability of a Liquid Jet," Phys. of Fluids, 13, 4, pp841-847, 1970

[8]D.B. Bogy. "Drop Formation in a Circular Liquid Jet," Ann. Rev. Fluid Mech., 11, pp207-228, 1979

[9]K.C. Chaudhary and L.G. Redekopp. "The Non-linear Capillary Instability of a Liquid Jet, Part I," J. Fluid Mech., 96, Part 2, pp257-274, 1980

[10]M. Orme and E.P. Muntz. "New Technique for Producing Highly Uniform Droplet Streams Over an Extended Range of Disturbance Wavenumbers," Rev. Sci. Instrum. 58, 2, pp279-284, 1987

[11]E.P. Muntz and M. Orme (Dixon). "Applications to Space for Free Flying Streams of Liquid Drops," J. of Spacecraft, 23, 4, pp411-419, 1986

[12]M. Orme (Dixon). "The Droplet Velocity Dispersion Device," AIAA Student Journal, Spring issue, pp14-23, 1985 and AIAA Preprint 85-0077

[13]B. Stanley. Du Pont Precision: private communication, March, 1988

[14]P. Huerre. "Effects of Friction and Heat Conduction on Sound Propagation in Ducts," Ph.D. Dissertation Department of Aeronautics & Astronautics, Stanford University, 1976

[15]G. Kirchhoff. "Ueber den Einfluss der Warmeleitung in einem Gase auf die Schallbewegund," Ann. Phys. Lpz., 134, pp172-193, 1868

[16]P.M. Morse and K.U. Ingard. "Theoretical Acoustics," McGraw Hill, New York, 1968

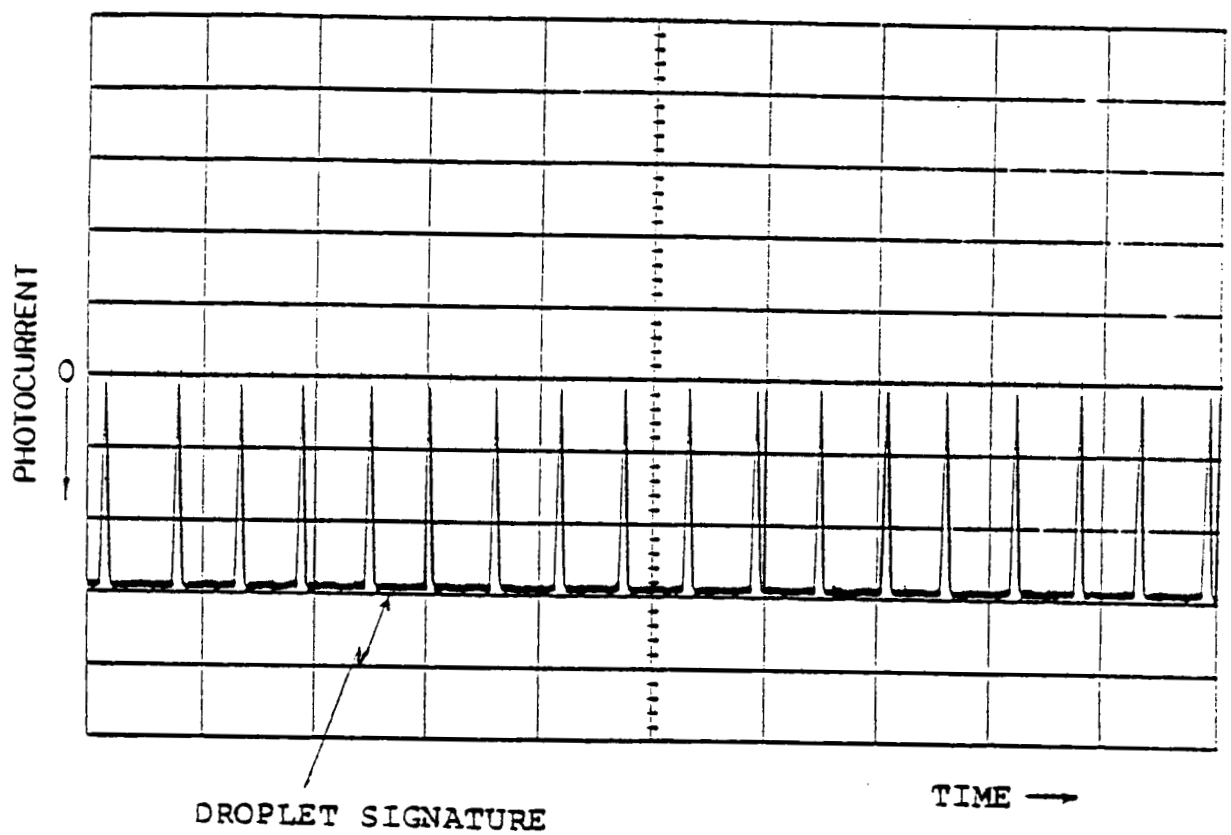

Figure 1: Droplet profile trace obtained by positioning the optical slit on the center of the droplet stream.

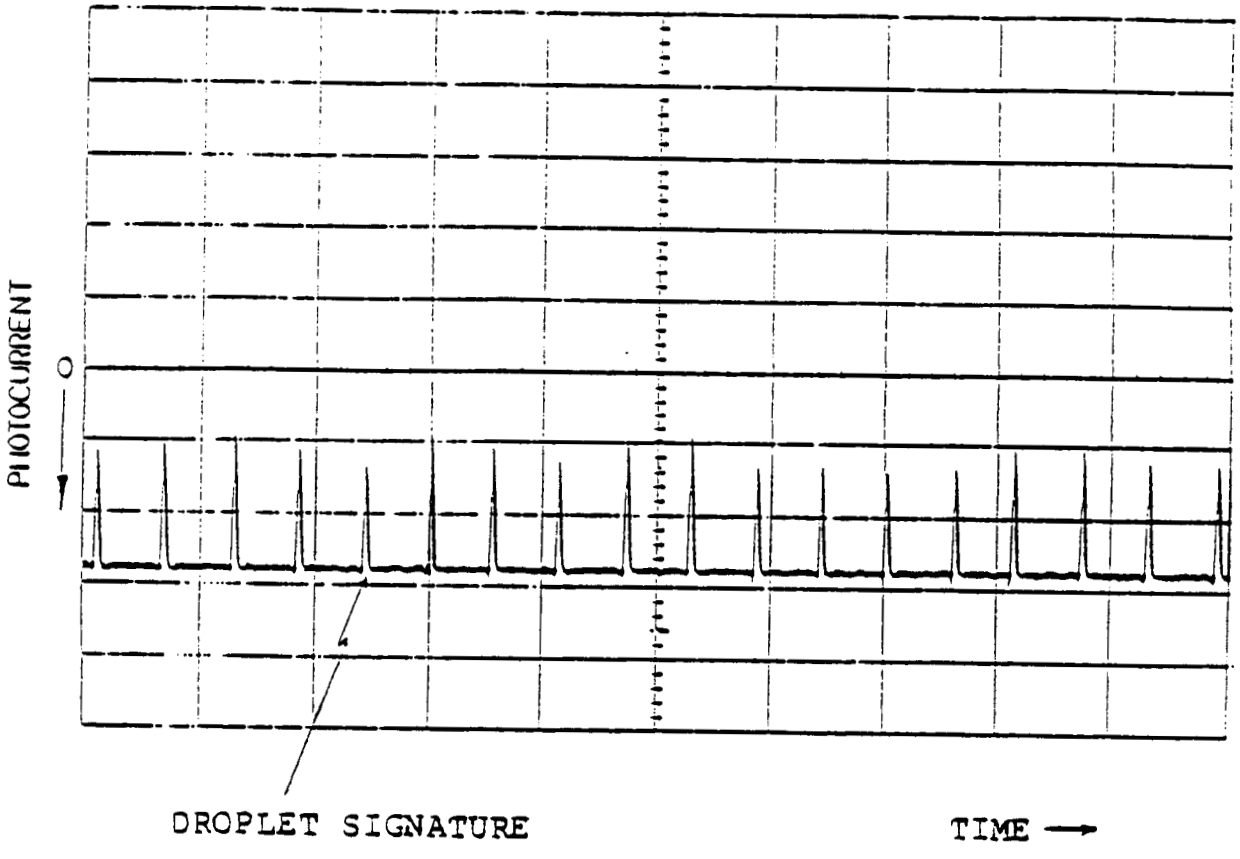

Figure 2: Droplet profile trace obtained by positioning the detector on the edge of the droplet stream in order to determine the angular dispersion of the stream.

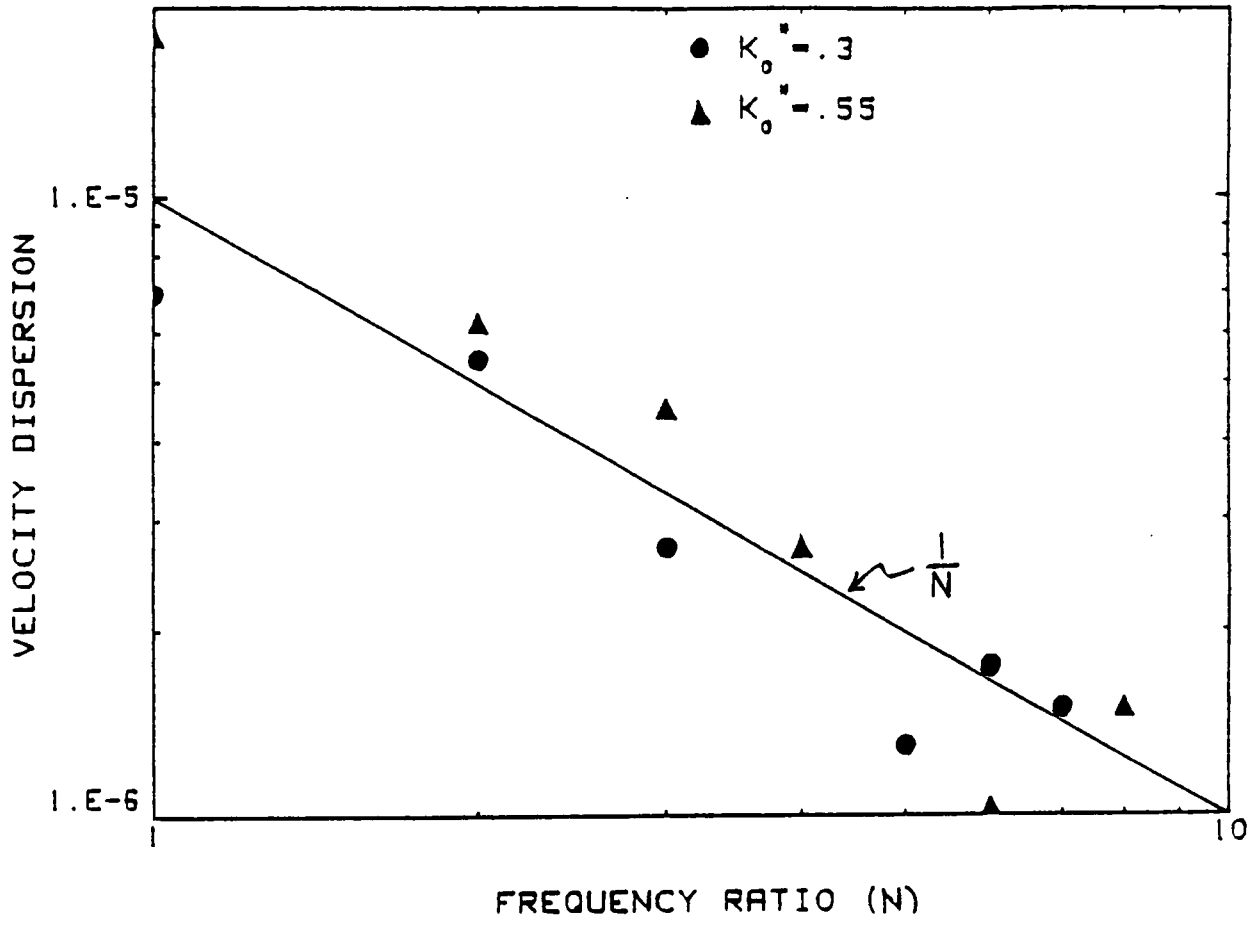

Figure 3: Response of the stream to an amplitude modulated disturbance. N is the frequency ratio. N=1 corresponds to a conventional constant amplitude sinusoidal waveform.

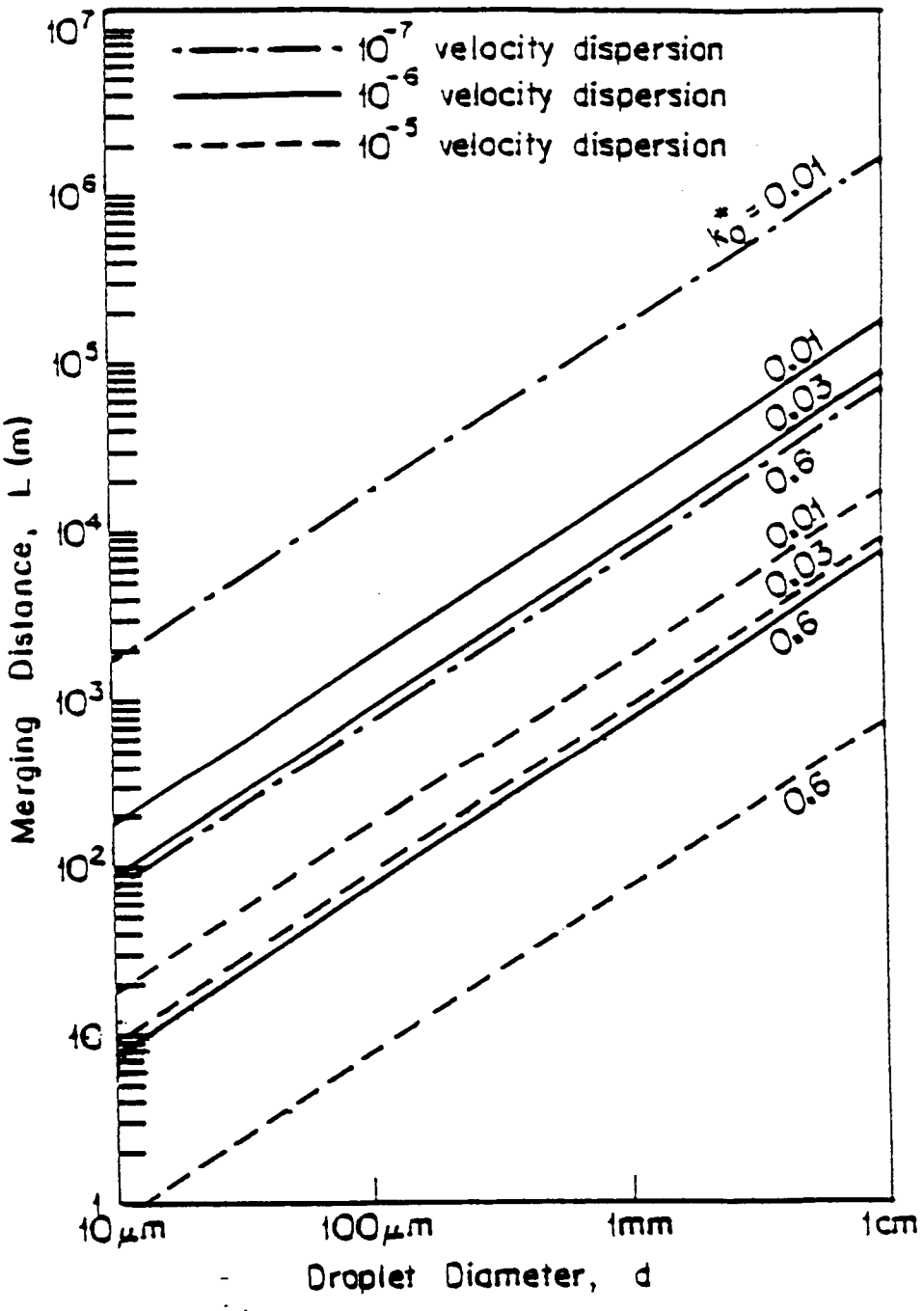

Figure 4: Distance a droplet stream can travel without significant merging with velocity dispersion and nondimensional wavenumber as parameters.

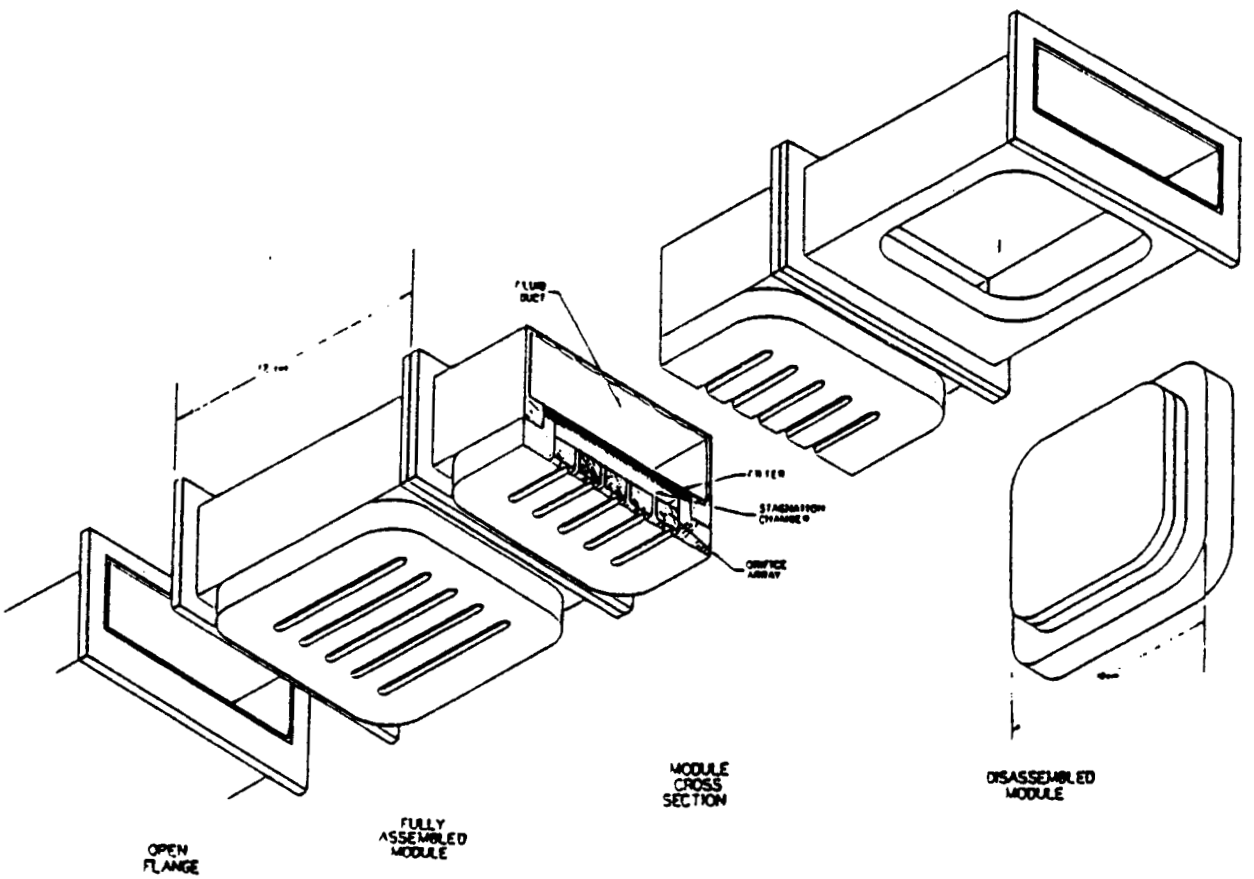

Figure 5: Schematic of assembly of several generator modules.

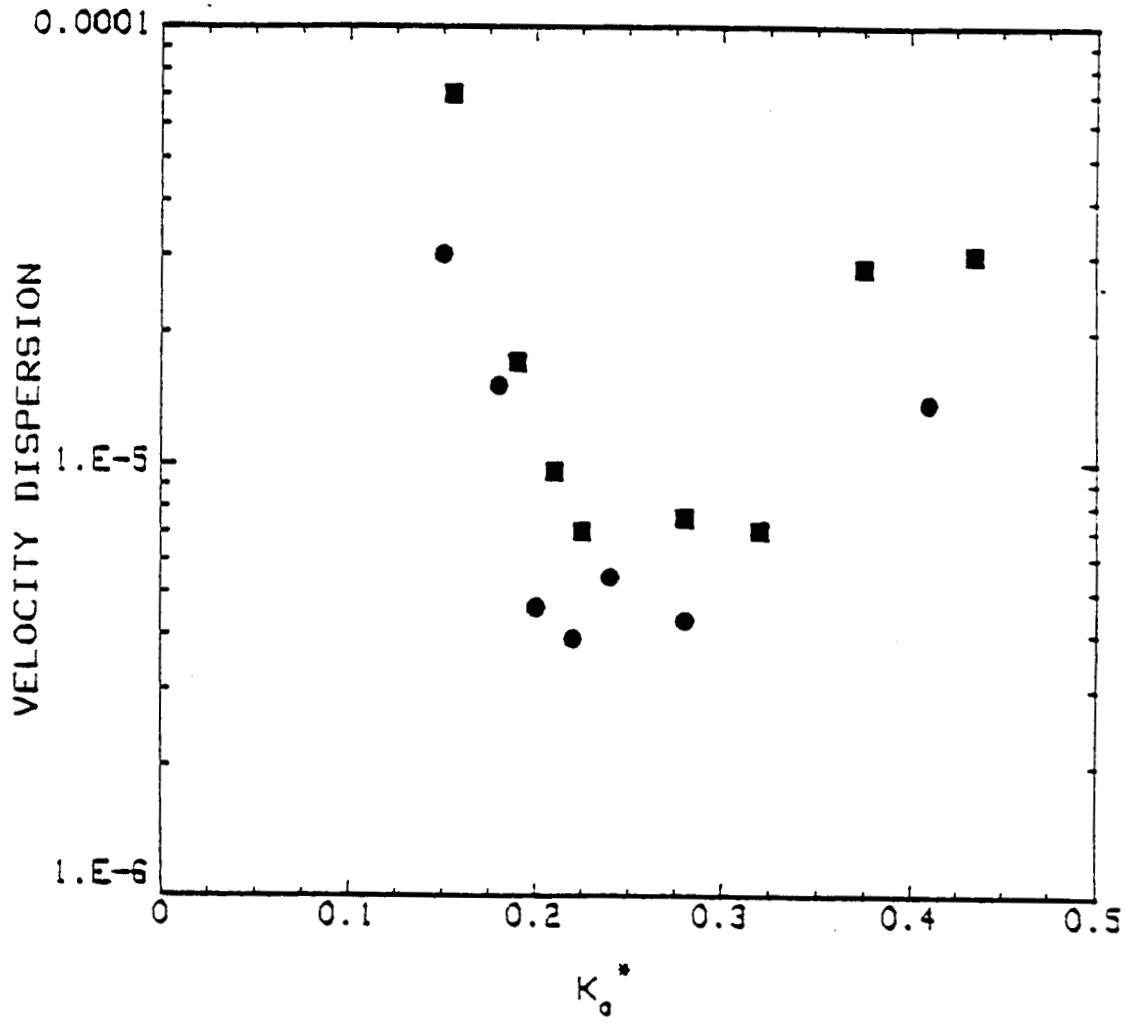

Figure 6: Behavior of a single stream when disturbed with the cavity disturbance mode of perturbation. Droplet fluid is DC-200: 1×10^{-5} m^2/s (10 cSt), nozzle diameter is 125 microns

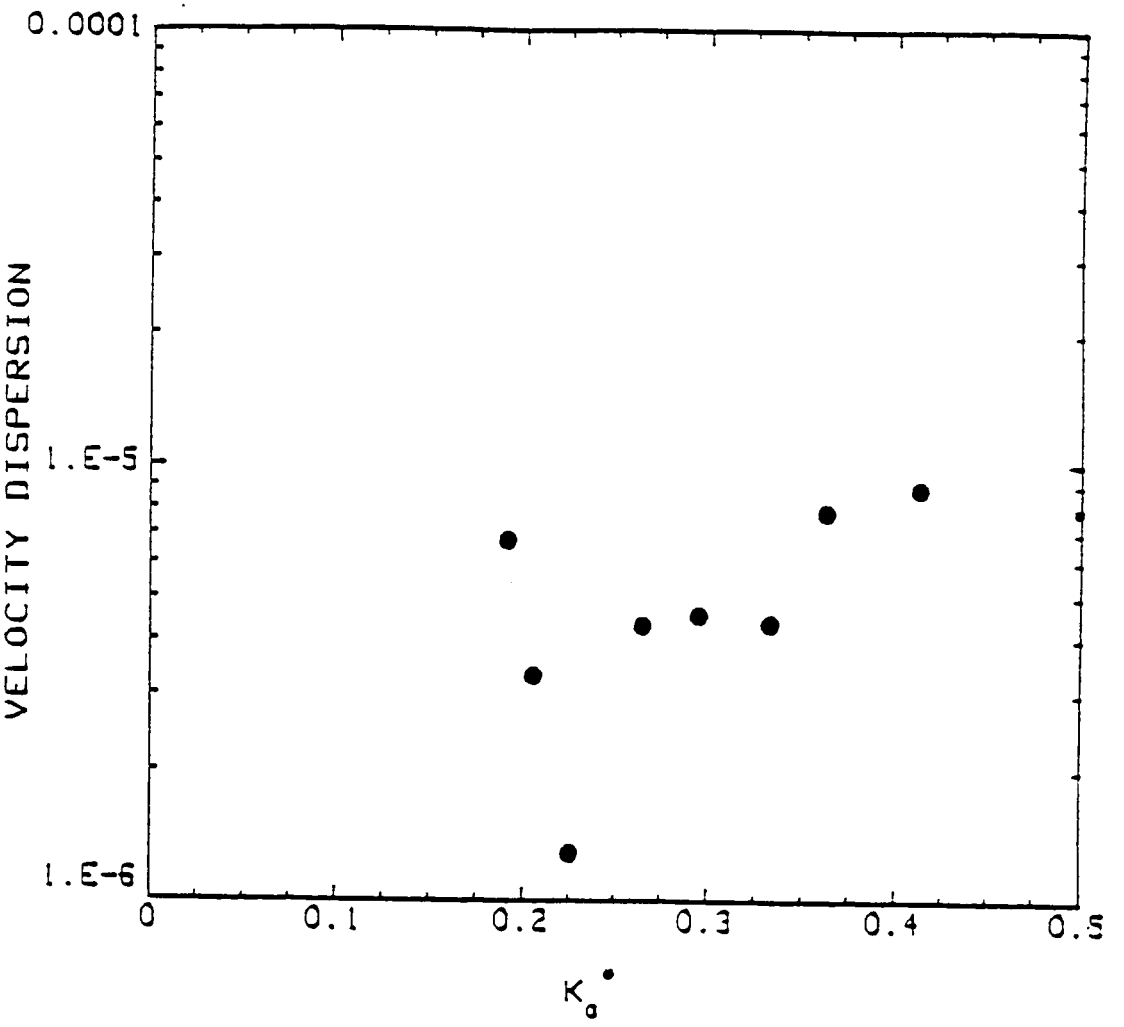

Figure 7: Behavior of a single stream when disturbed with the orifice disturbance mode of perturbation. Droplet fluid is DC-200: $1x10^{-5}$ m^2/s (10 cSt) , nozzle diameter is 125 microns

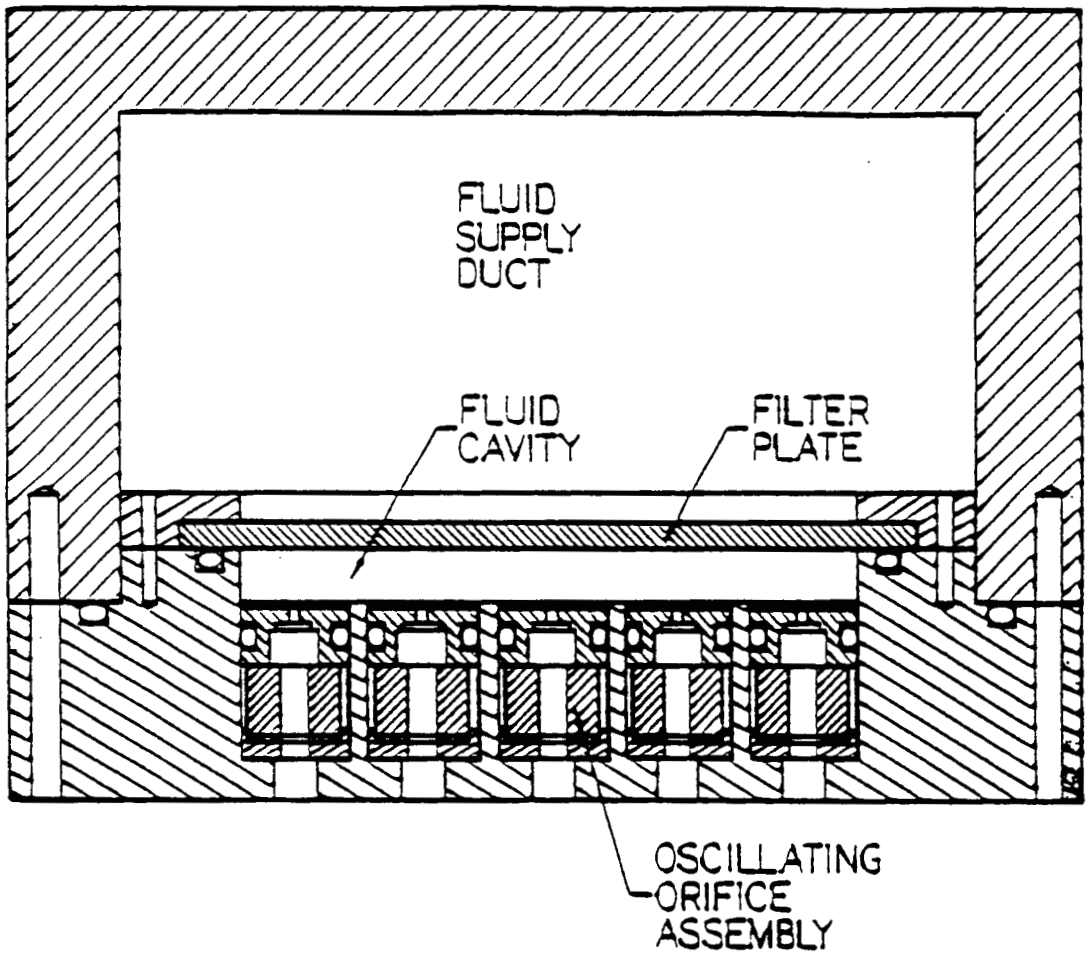

Figure 8: Schematic of cross-section of generator module illustrating means of perturbation chosen for present design.

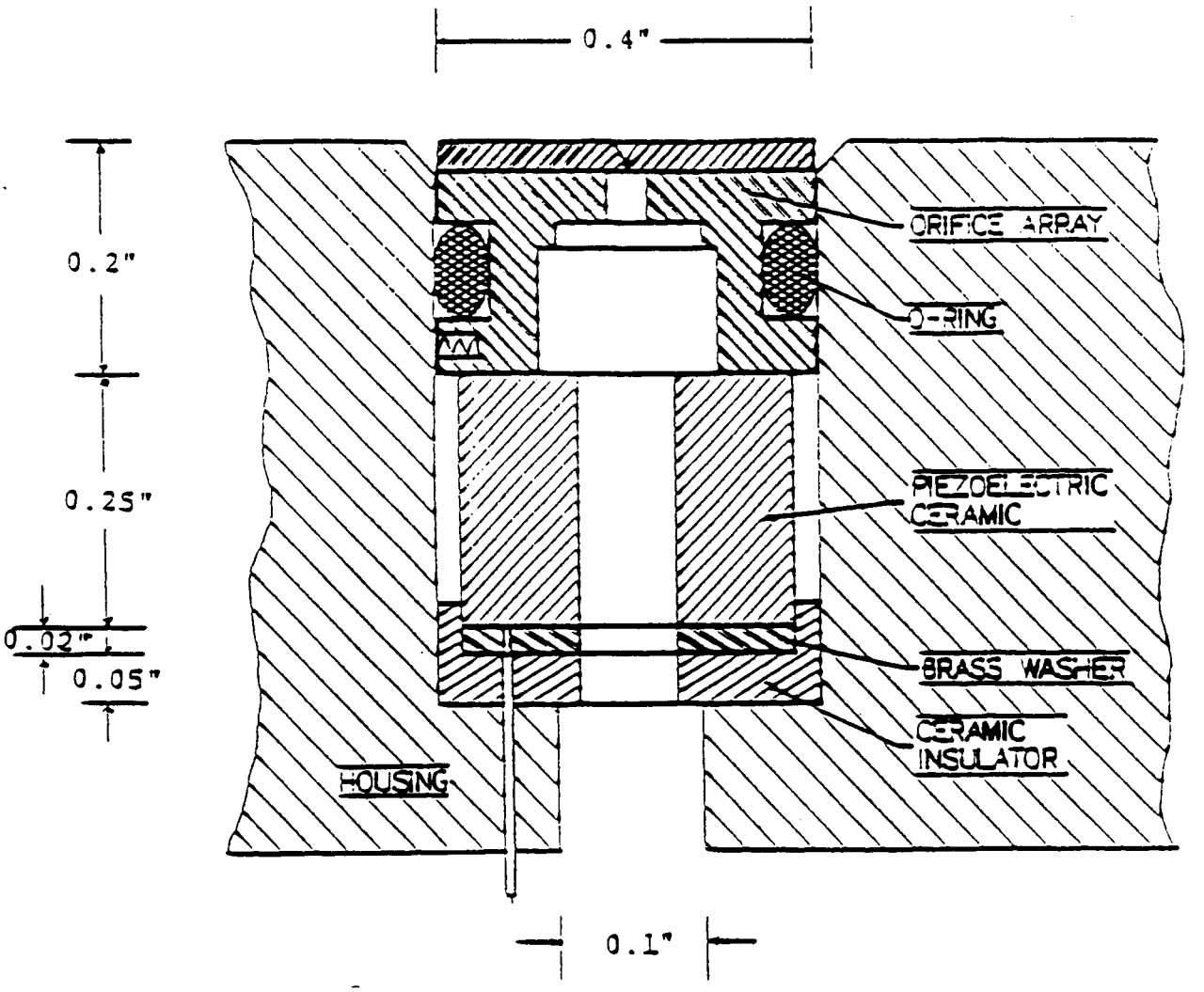

Figure 9: Schematic of the details of orifice array assembly.

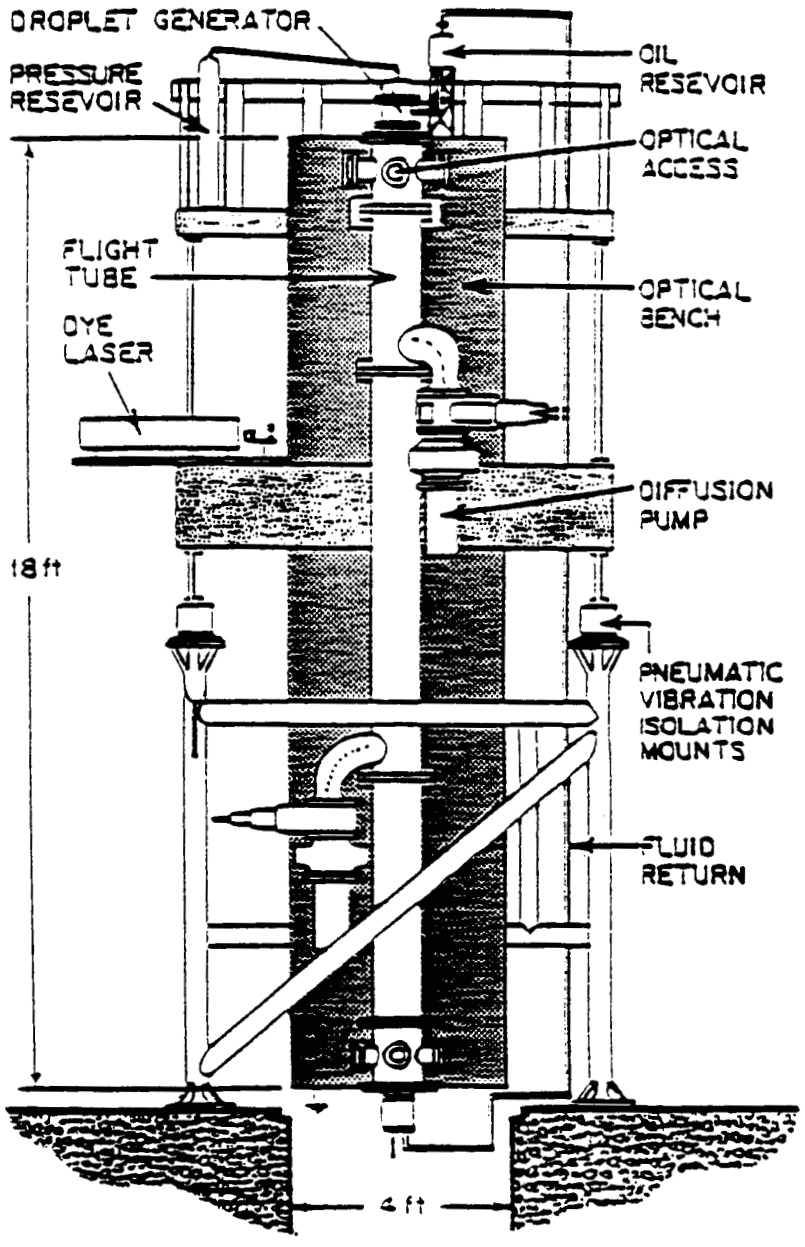

Figure 10: Schematic of the apparatus used to test the multi-stream droplet generator: Droplet Dynamics Space Simulator.

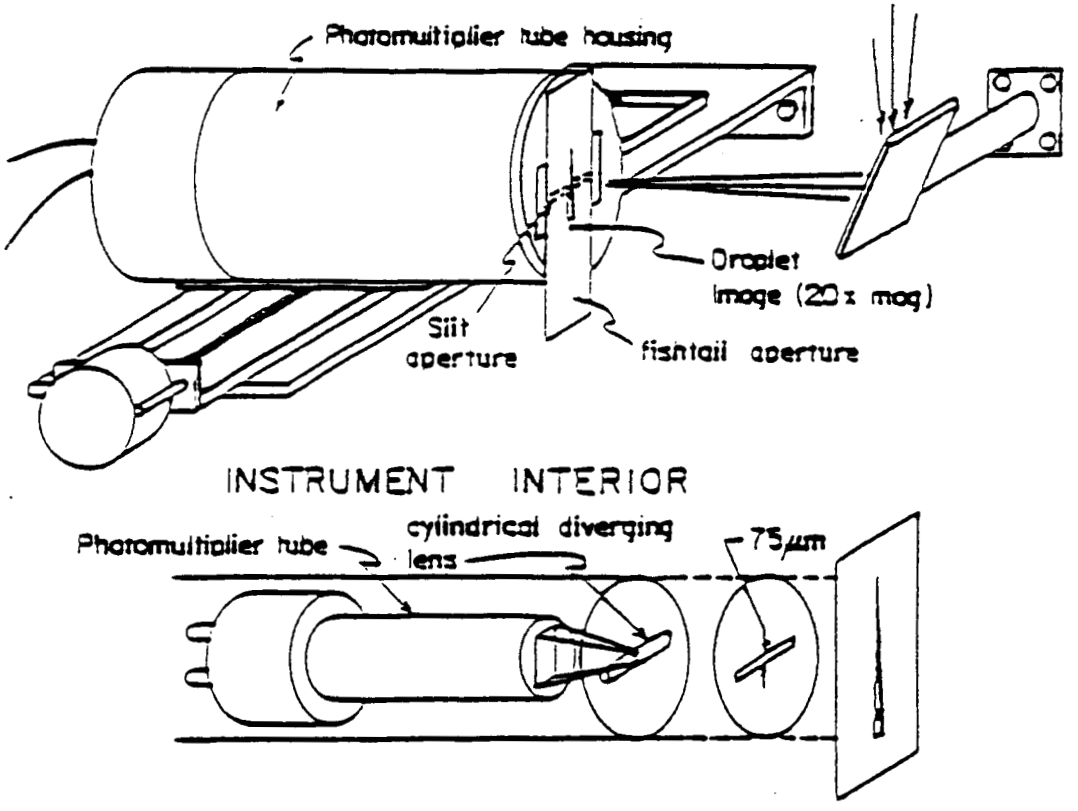

Figure 11: Detector used to observe the droplet streams.

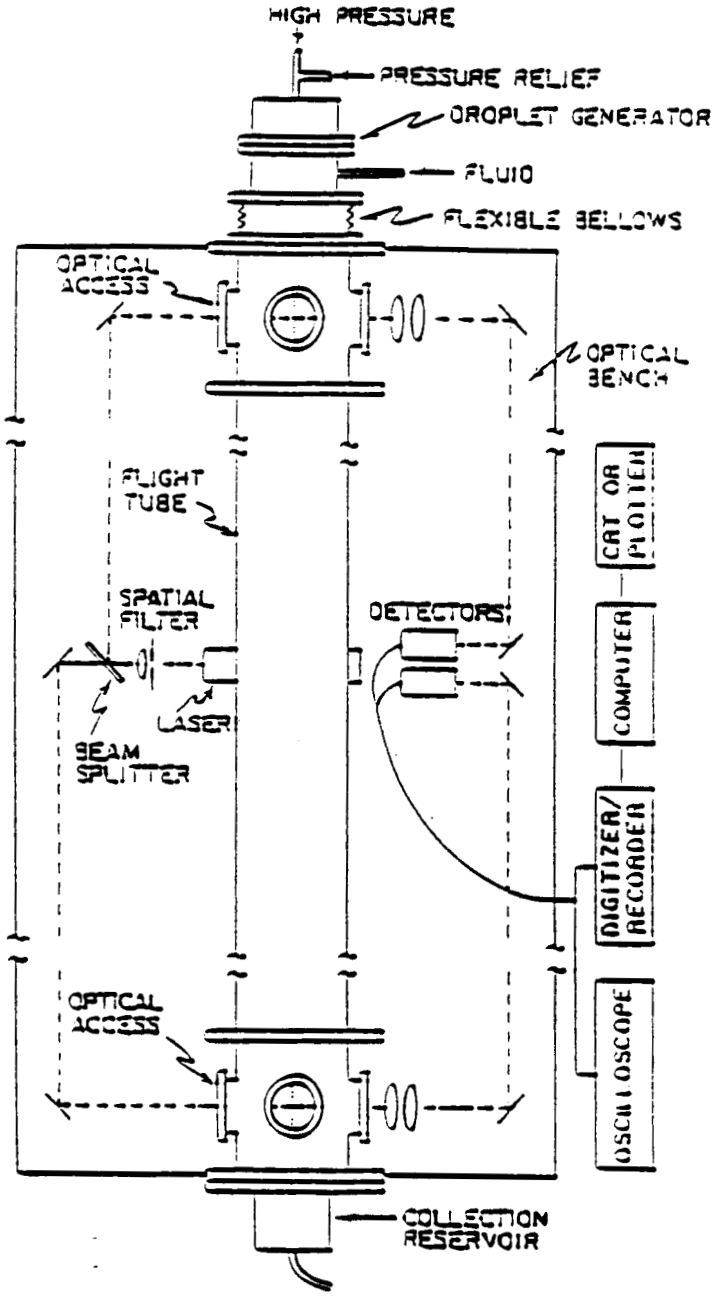

Figure 12: Schematic of optical path and data retrieval methods.

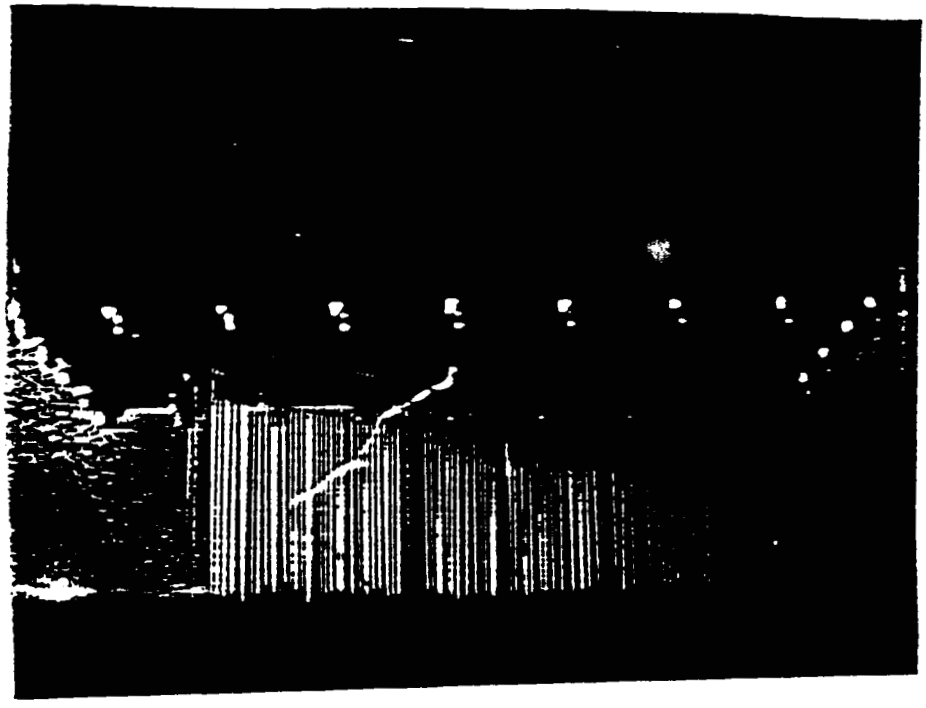

Figure 13: Photograph illustrating the generator performance with the 100 hole array which was manufactured by Du Pont Precision.

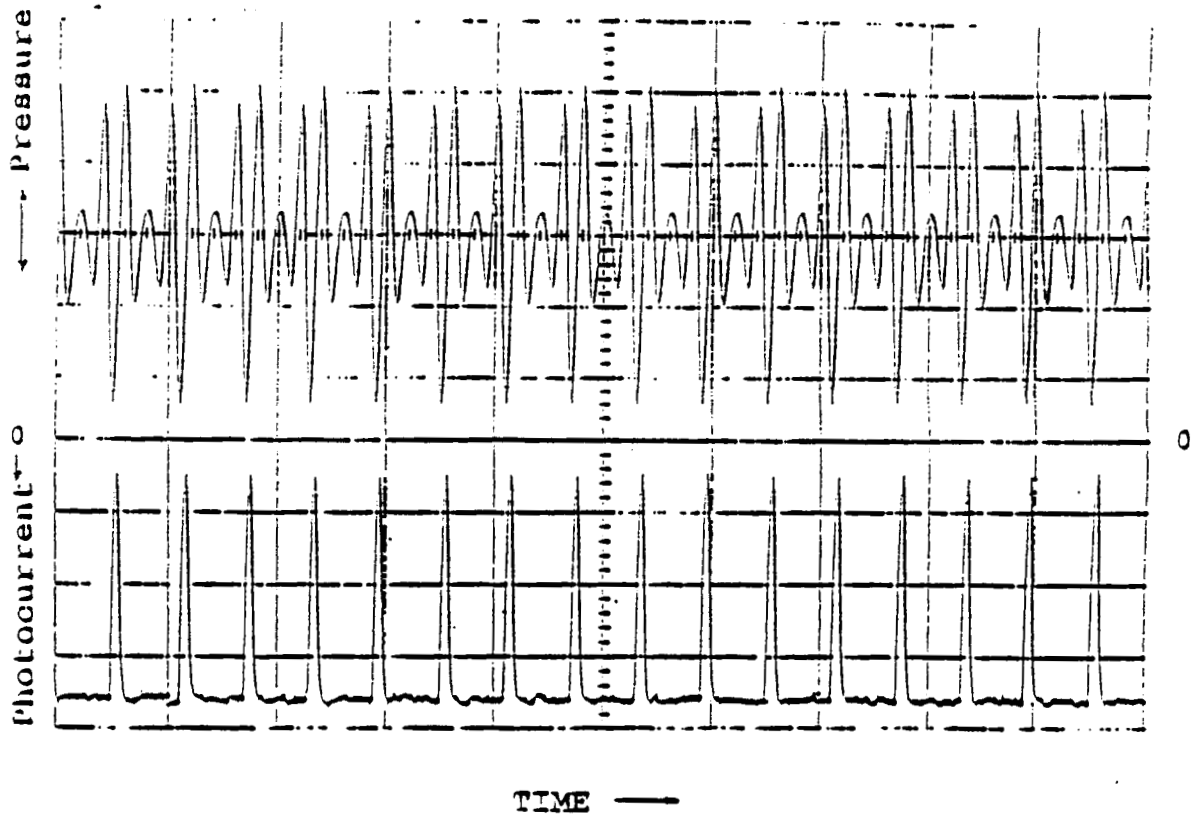

Figure 14: Droplet stream waveform (lower trace) and perturbation waveform (upper trace) obtained from the 100 hole Du Pont Array.

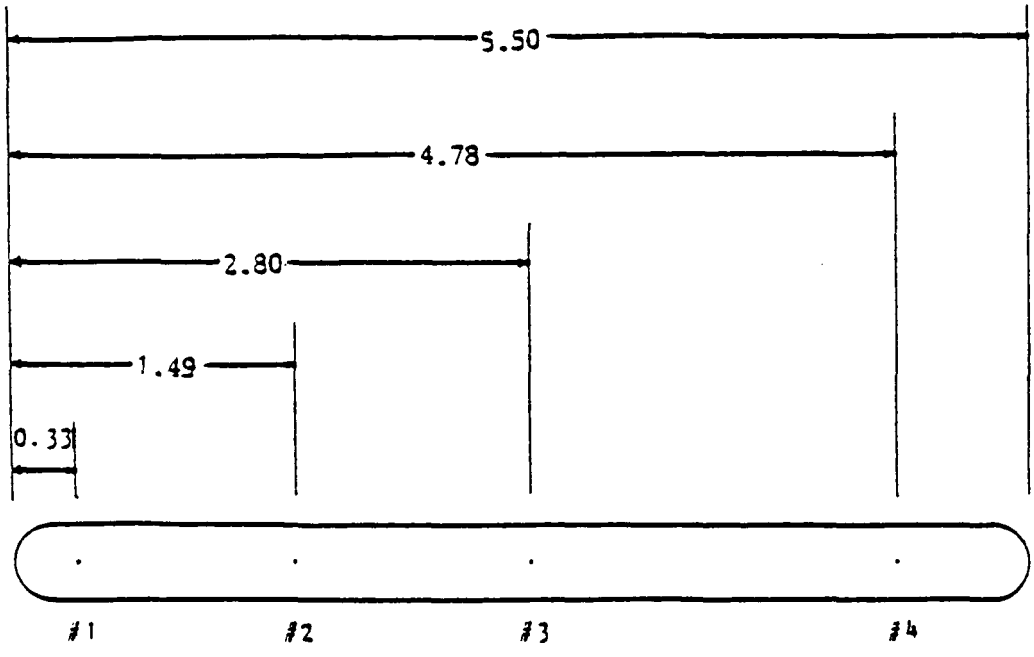

Figure 15: Schematic of four hole NASA Lewis array.

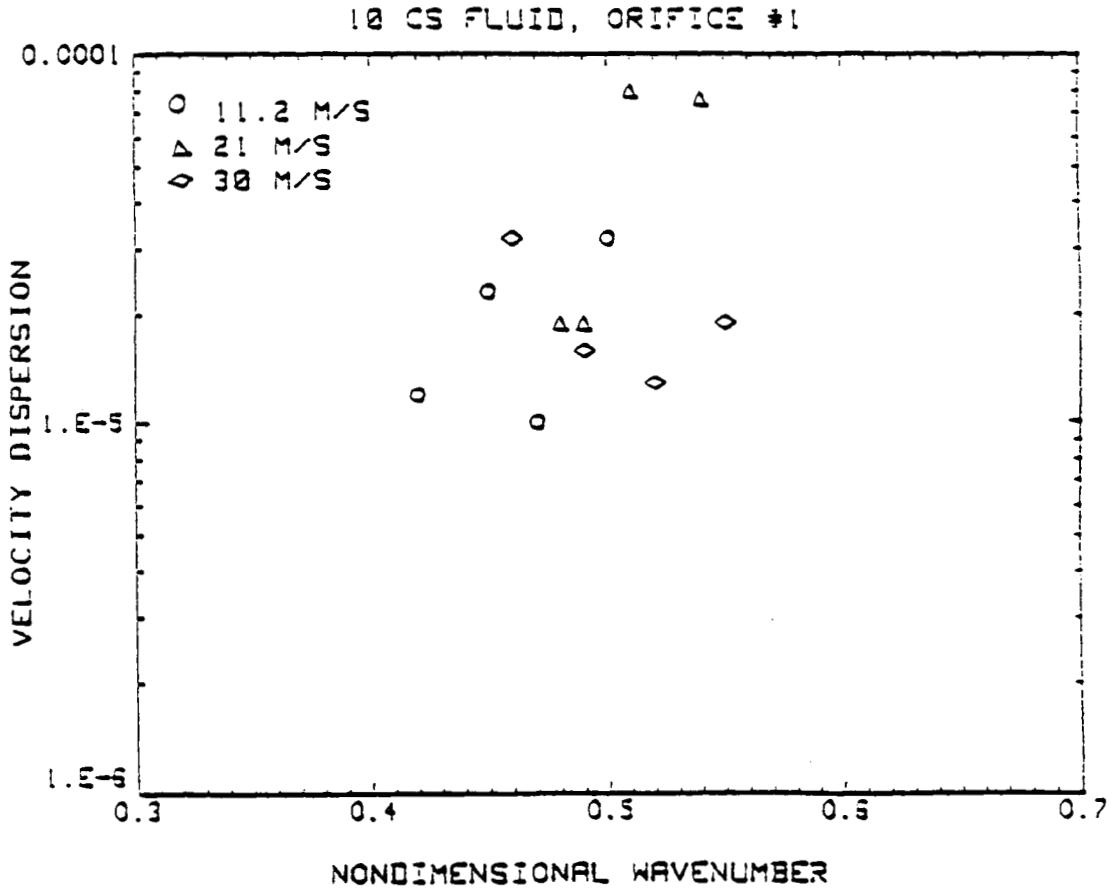

Figure 16: Velocity dispersions as a function of non-dimensional wavenumber for streams generated from orifice #1 of the NASA Lewis array with $1x10^{-6}$ m^2/s (10 cSt) DC-200.

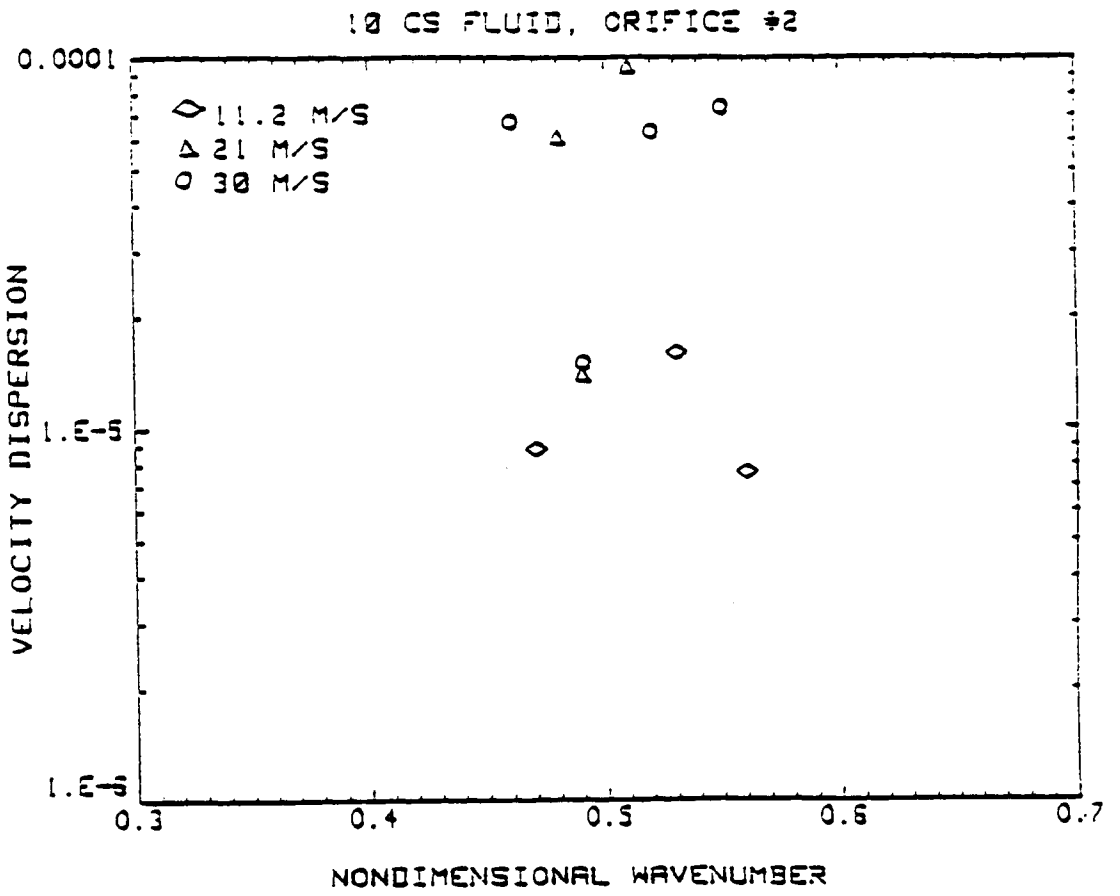

Figure 17: Velocity dispersions as a function of non-dimensional wavenumber for streams generated from orifice #2 of the NASA Lewis array with $1x10^{-6}$ m^2/s (10 cSt) DC-200.

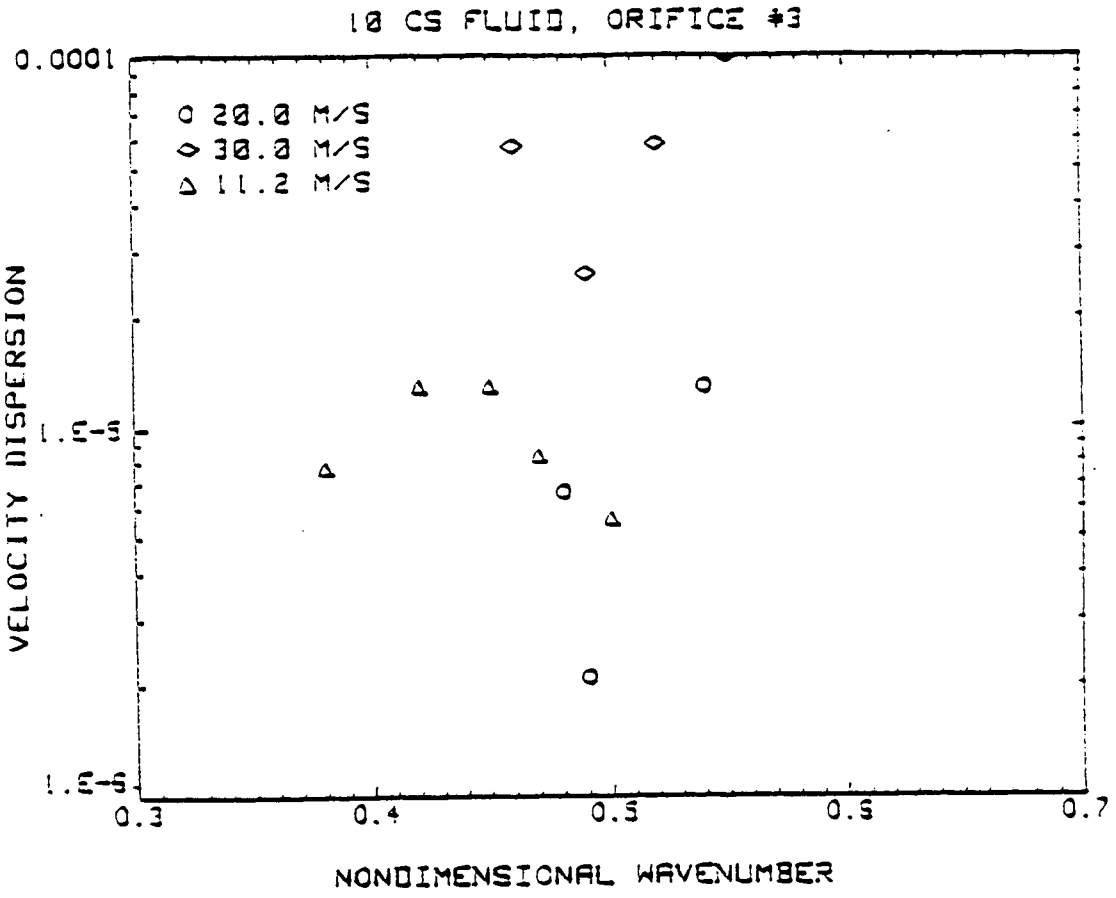

Figure 18: Velocity dispersions as a function of non-dimensional wavenumber for streams generated from orifice #3 of the NASA Lewis array with $1x10^{-5}$ m^2/s (10 cSt) DC-200.

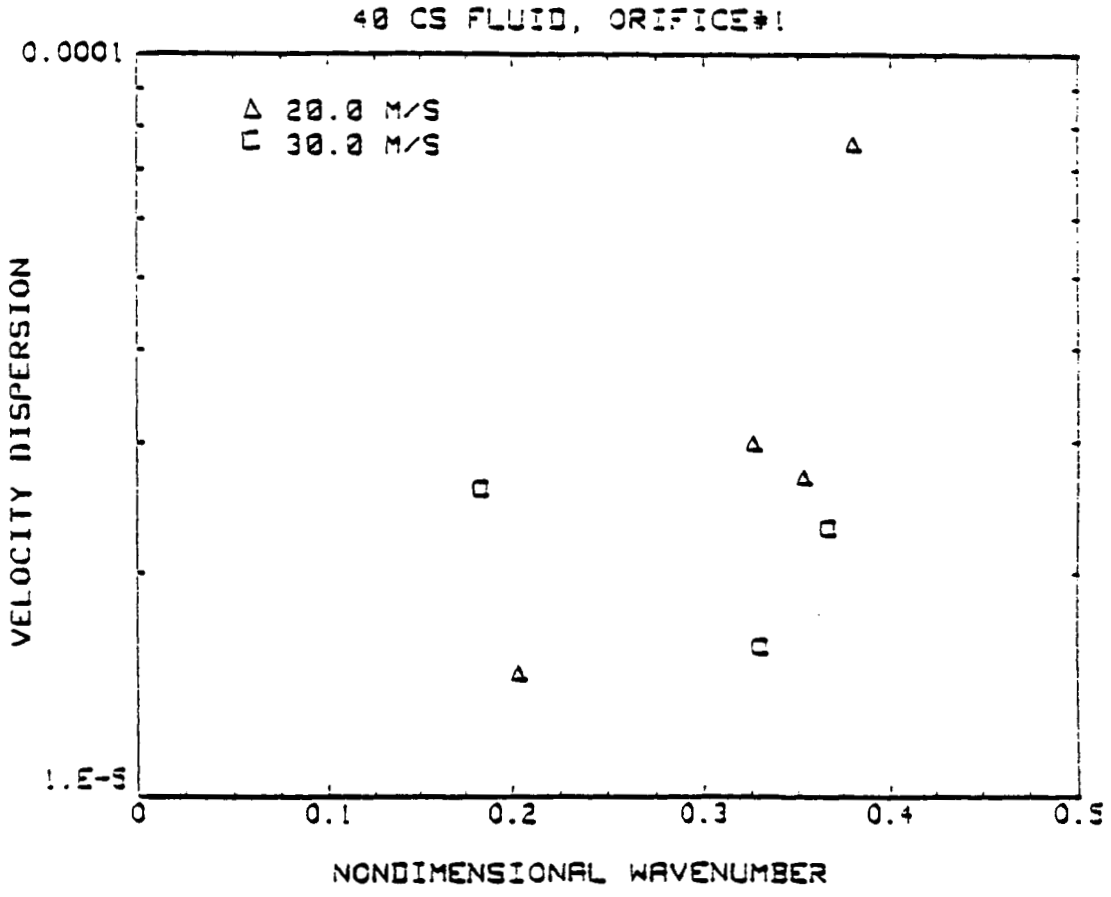

Figure 19: Velocity dispersions as a function of non-dimensional wavenumber for streams generated from orifice #1 of the NASA Lewis array with 4×10^{-5} m^2/s (40 cSt) DC-200.

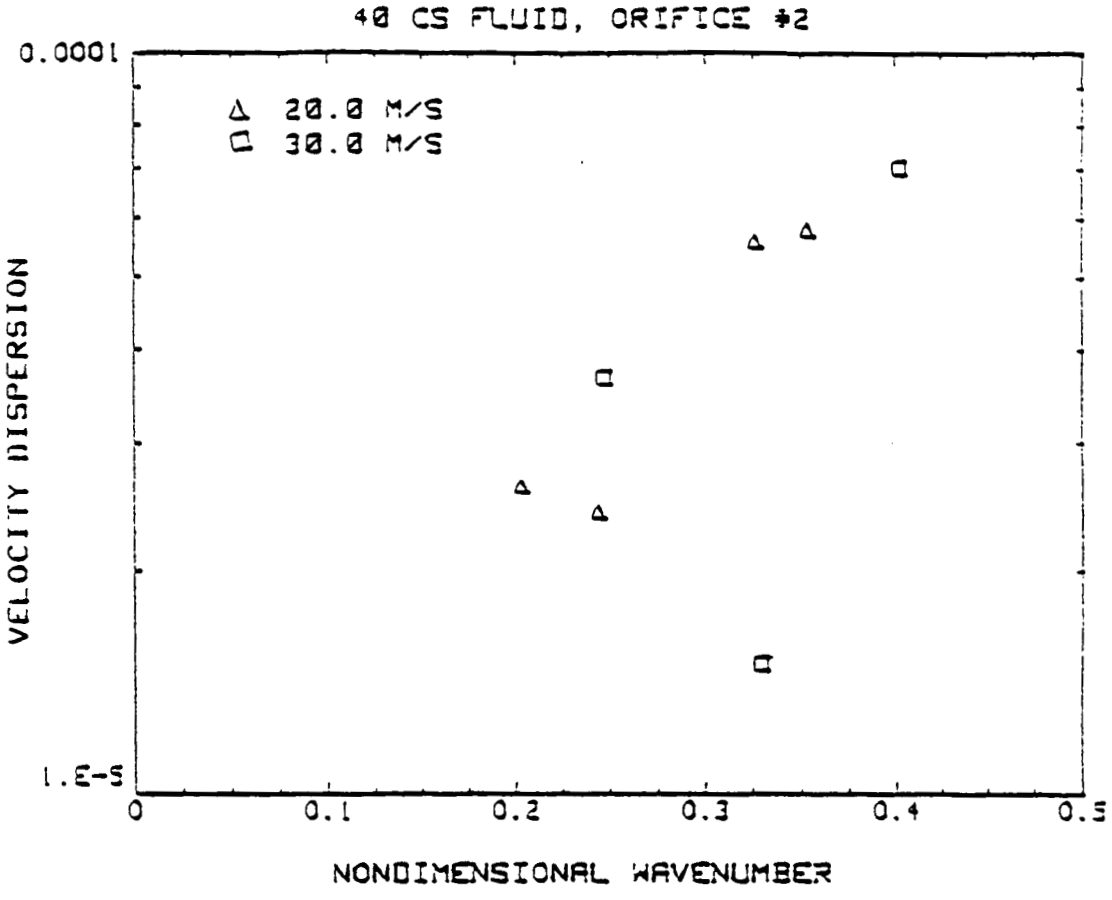

Figure 20: Velocity dispersions as a function of non-dimensional wavenumber for streams generated from orifice #2 of the NASA Lewis array with $4x10^{-6}$ m^2/s (40 cSt) DC-200.

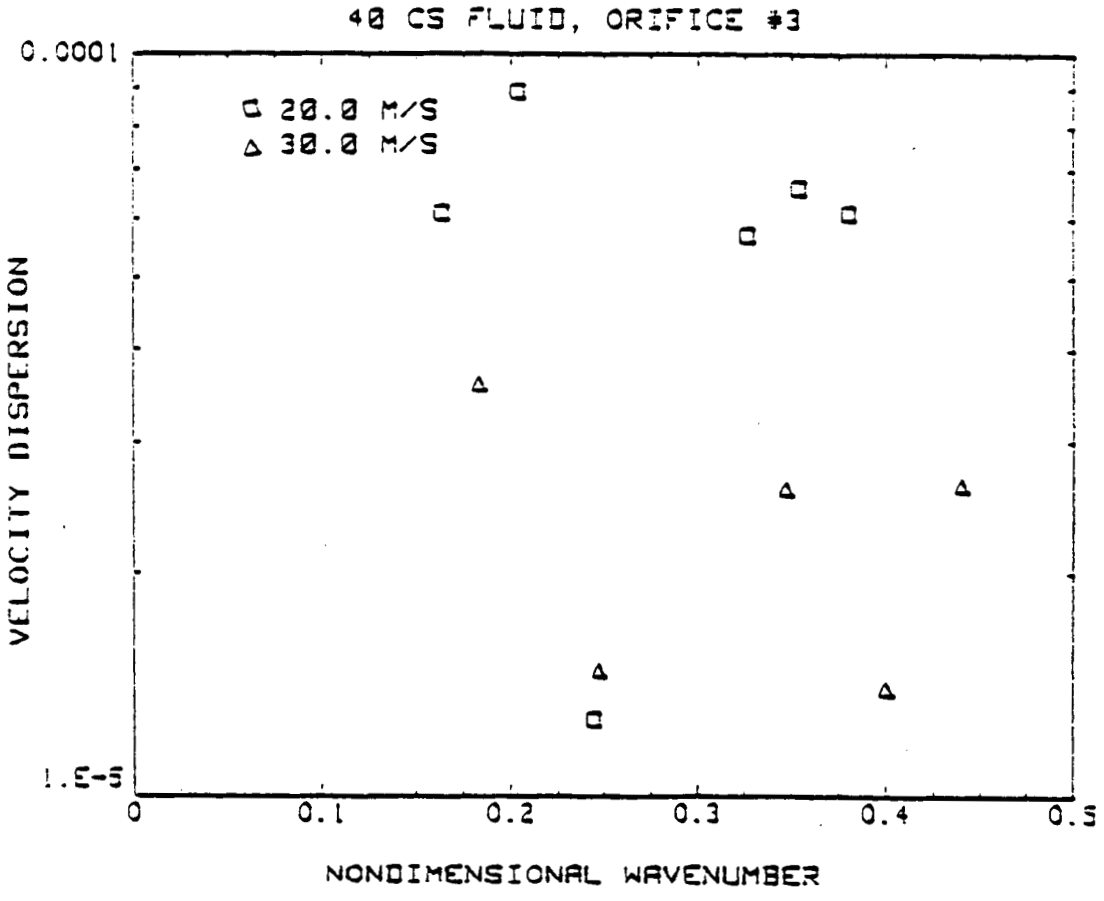

Figure 21: Velocity dispersions as a function of non-dimensional wavenumber for streams generated from orifice #3 of the NASA Lewis array with $4x10^{-5}$ m^2/s (40 cSt) DC-200.

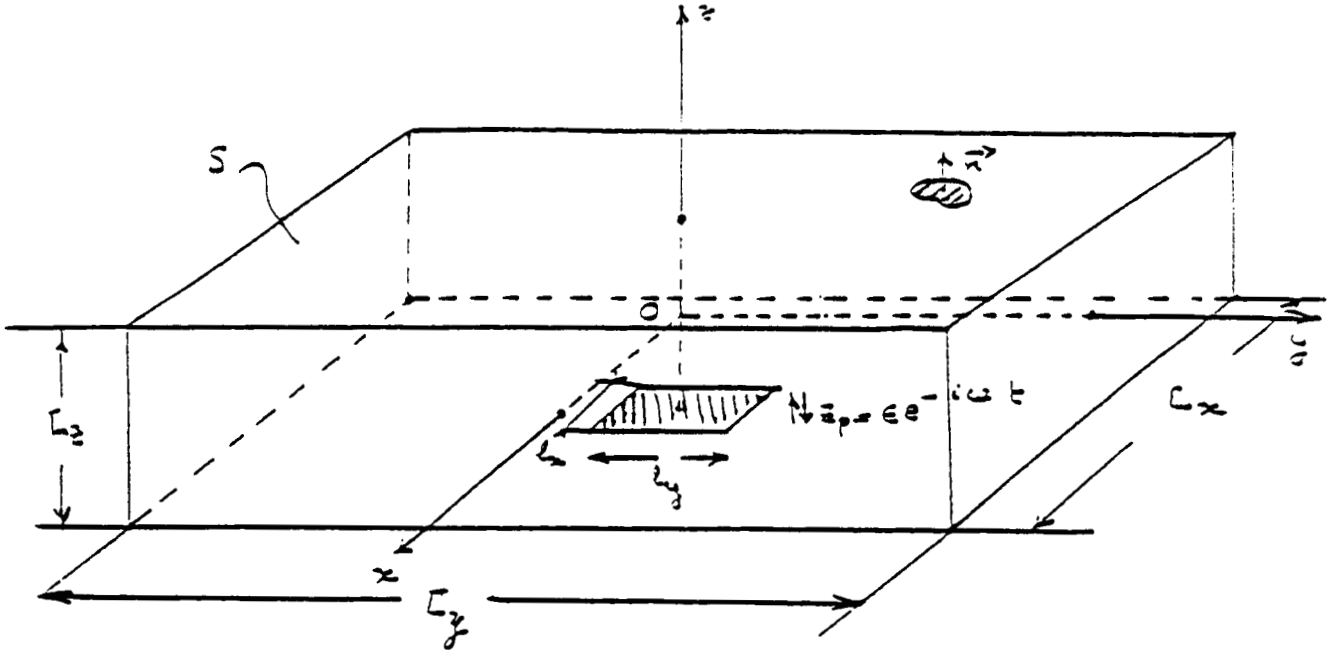

Figure 22: General configuration for acoustic analysis.

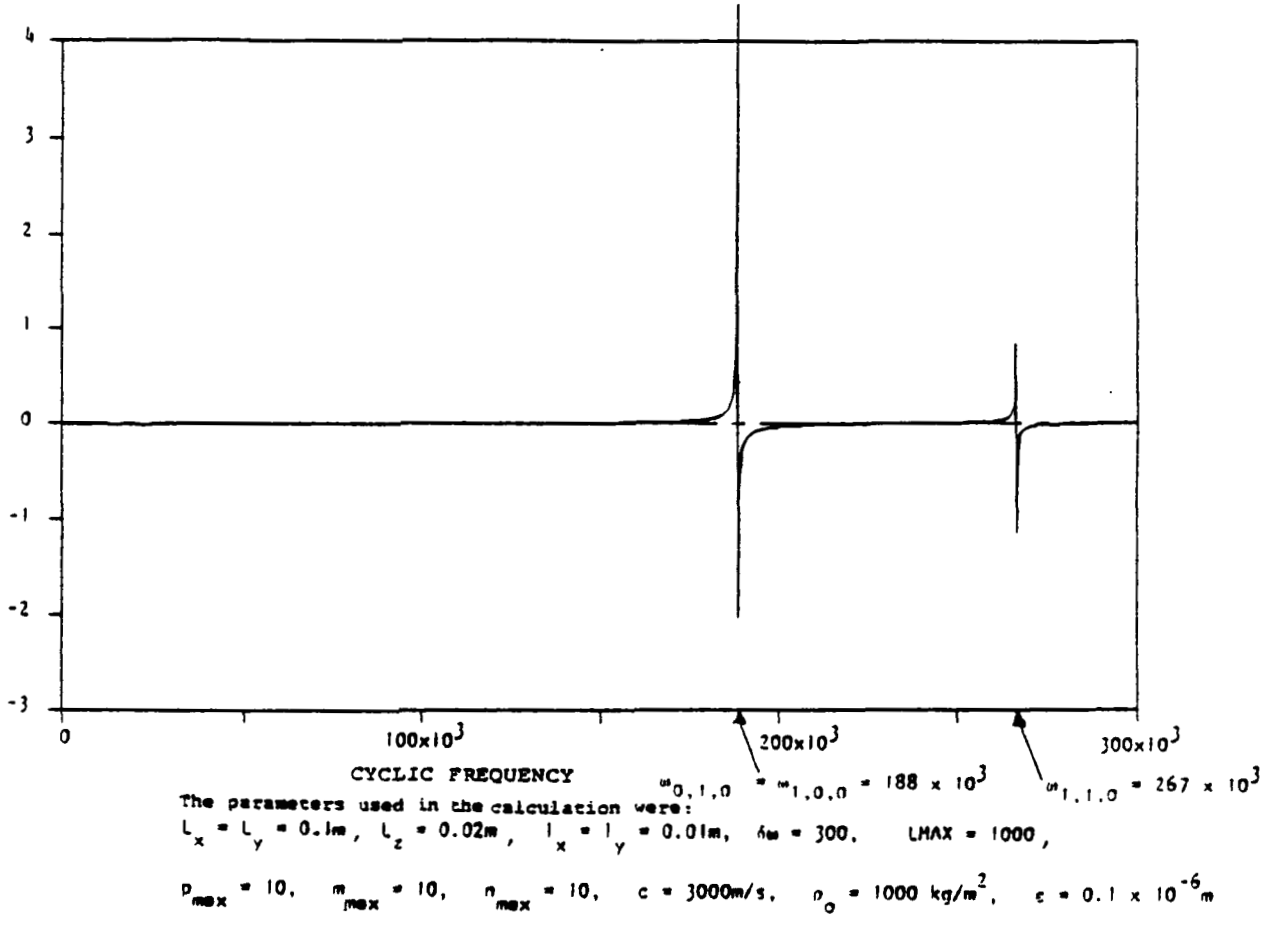

Figure 23: Results of acoustic analysis.

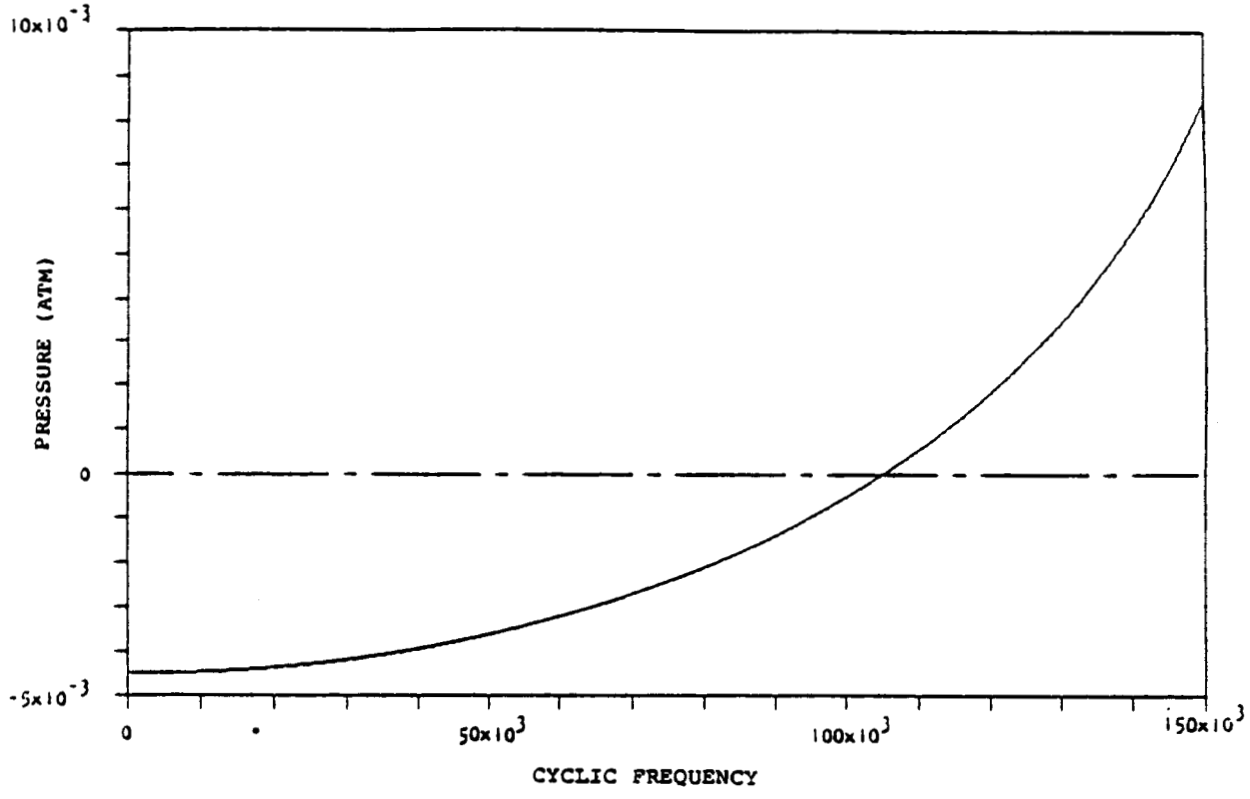

Figure 24: Results of acoustic analysis.

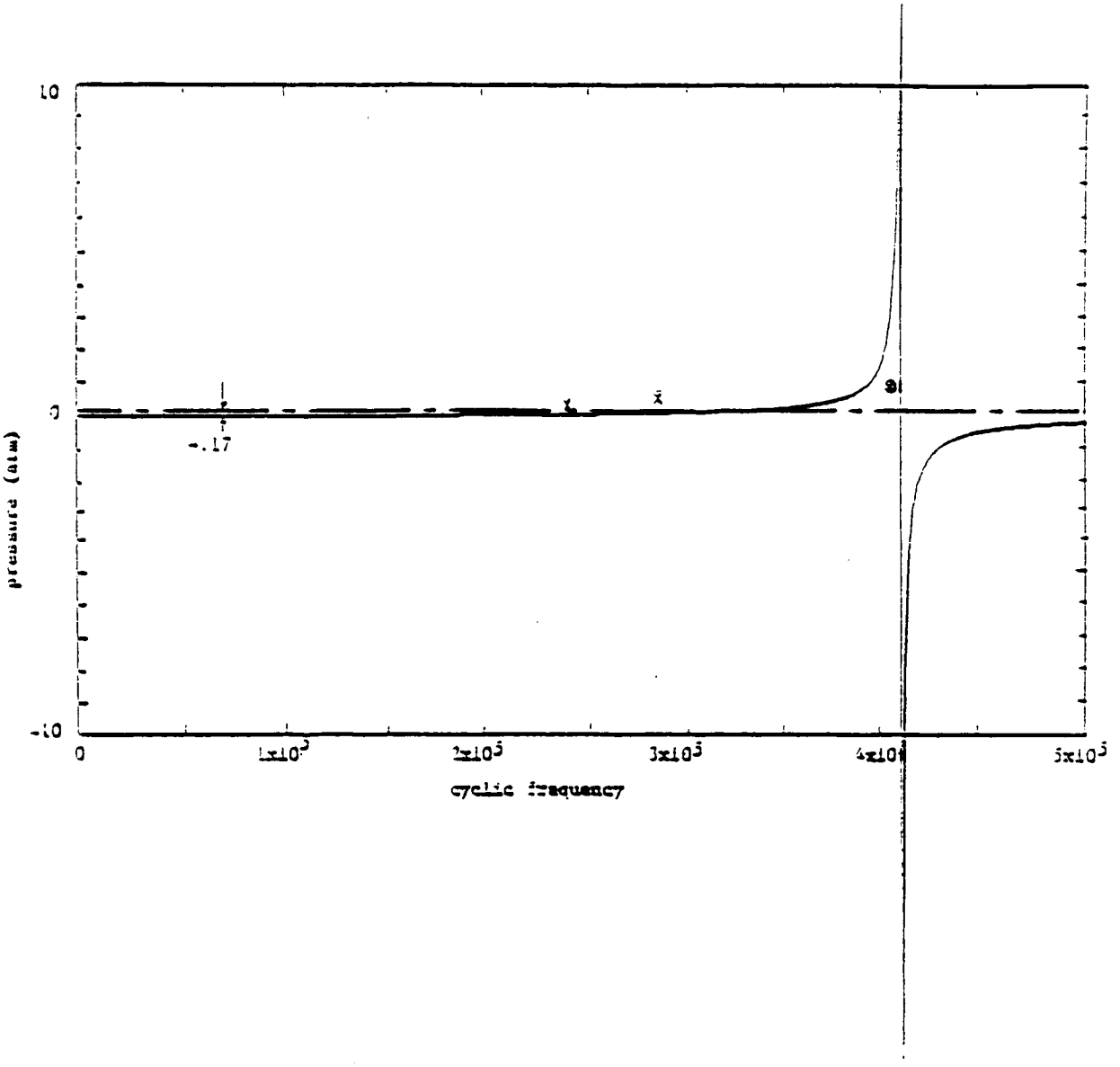

Figure 25: Prediction of cavity pressure as a function of frequency for the cavity disturbance mode of operation. Experimental points are absolute values since no documentation of phase was made.

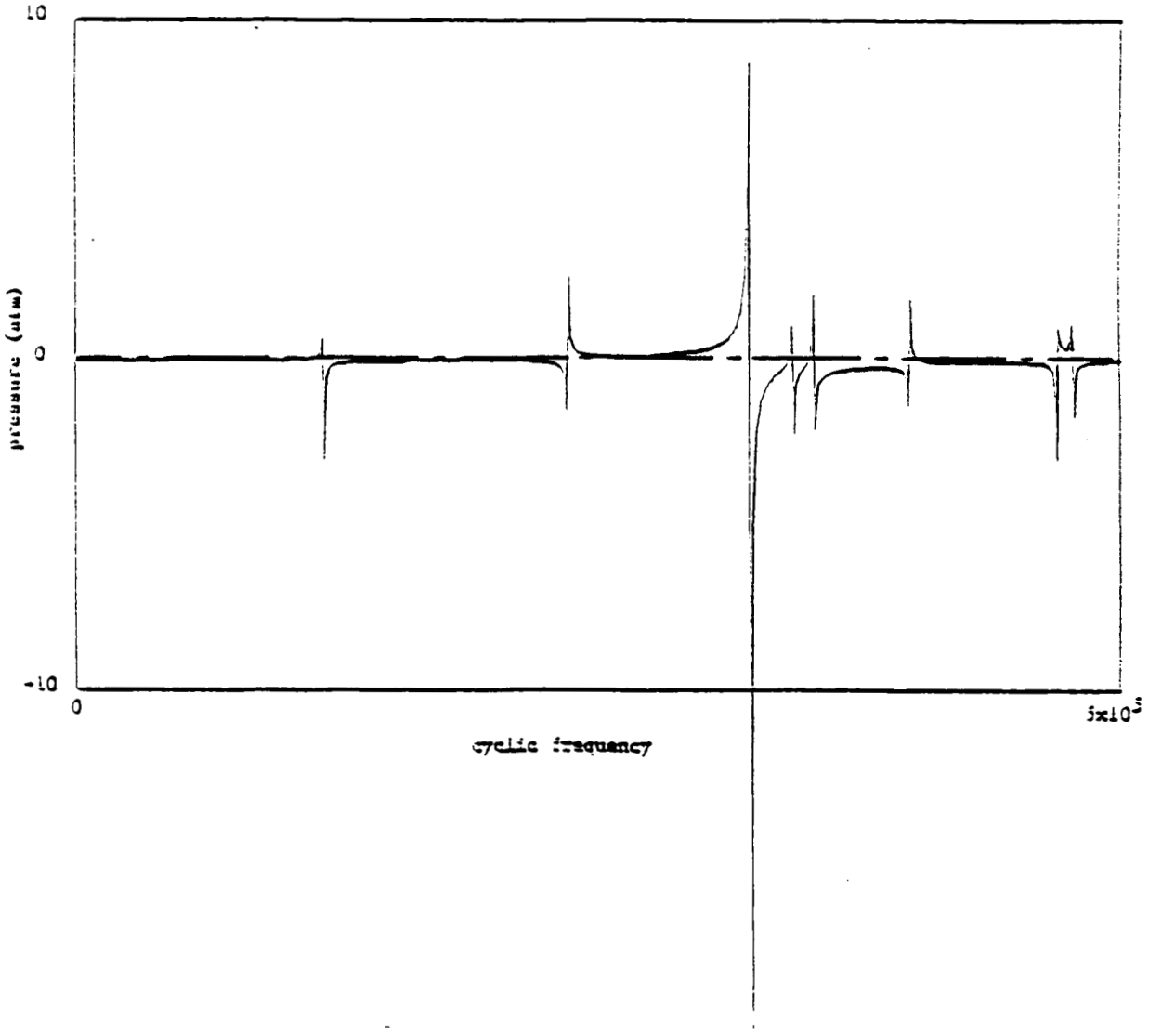

Figure 26: Prediction of cavity pressure as a function of frequency for the multi-stream generator with a single large cavity.

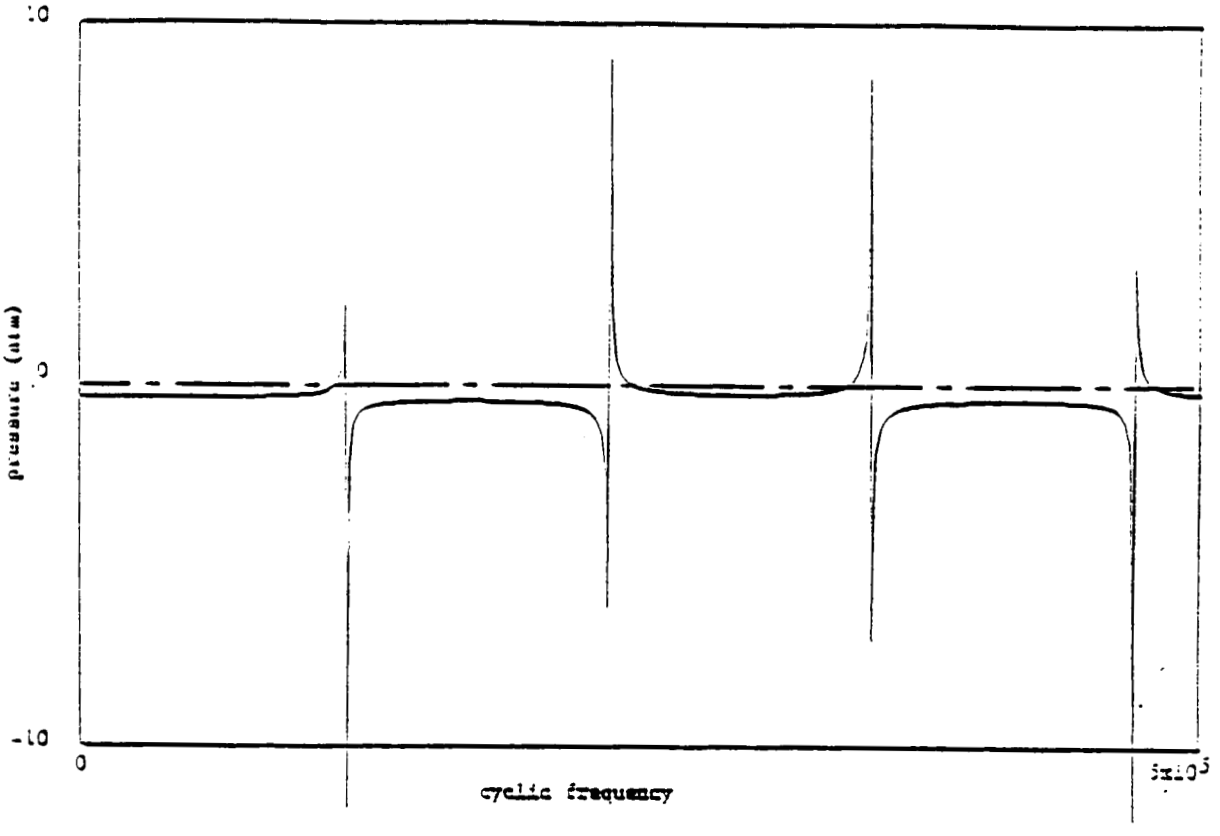

Figure 27: Prediction of cavity pressure as a function of frequency for the generator configuration of five separate cavities; one for each array.

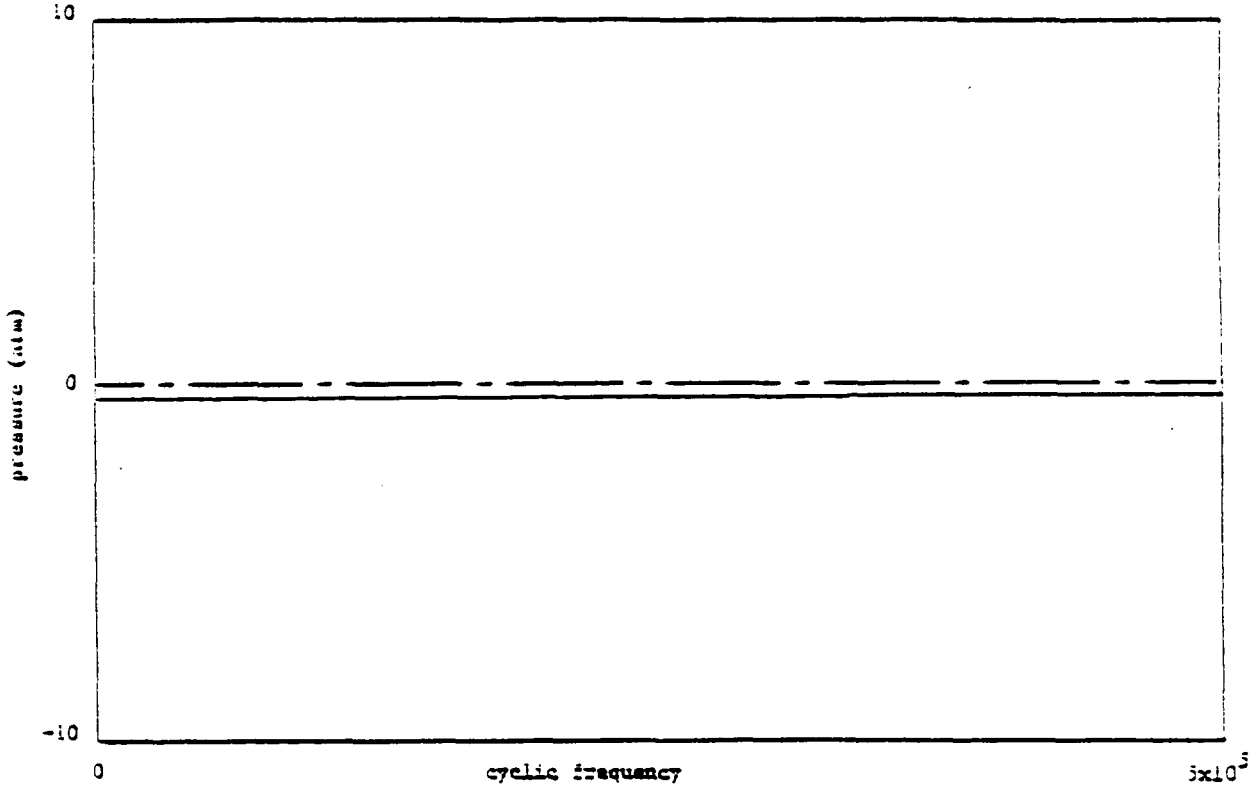

Figure 28: Prediction of cavity pressure as a function of frequency for the generator configuration of 20 separate cavities, four cavities to one array.

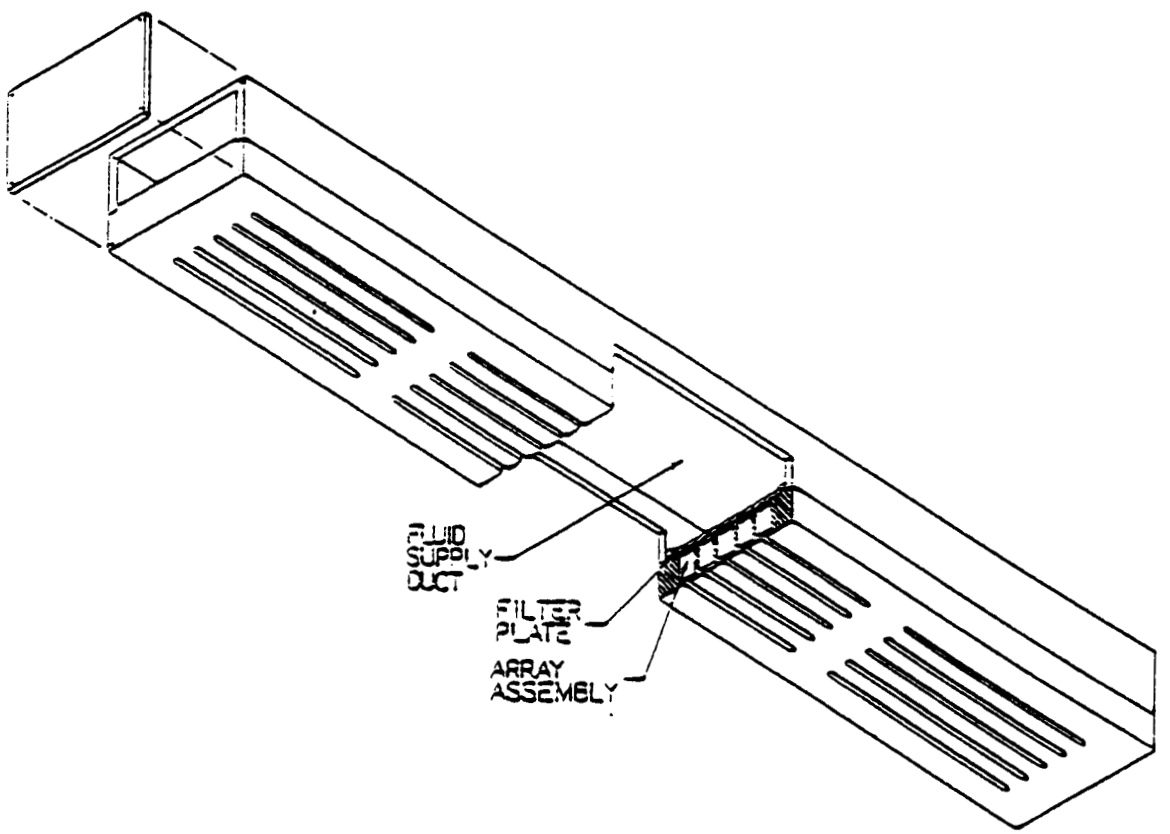

Figure 29: Schematic of nominal 5000-orifice droplet generator.

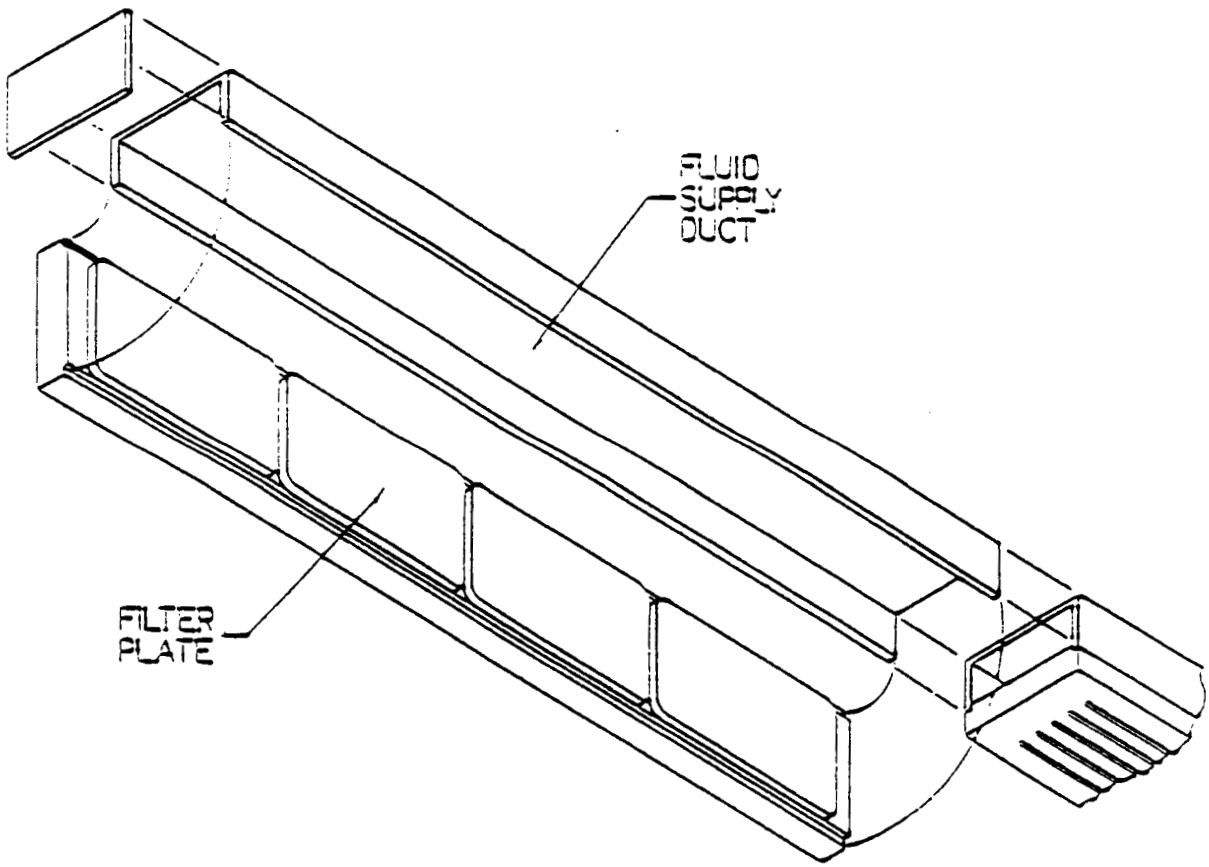

Figure 30: Schematic of generator illustrating configuration.

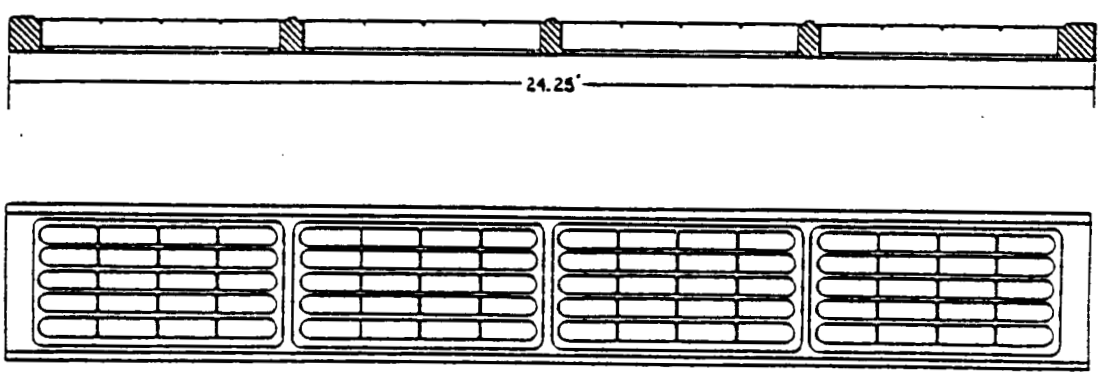

Figure 31: Schematic of top view and bottom view of array holder.

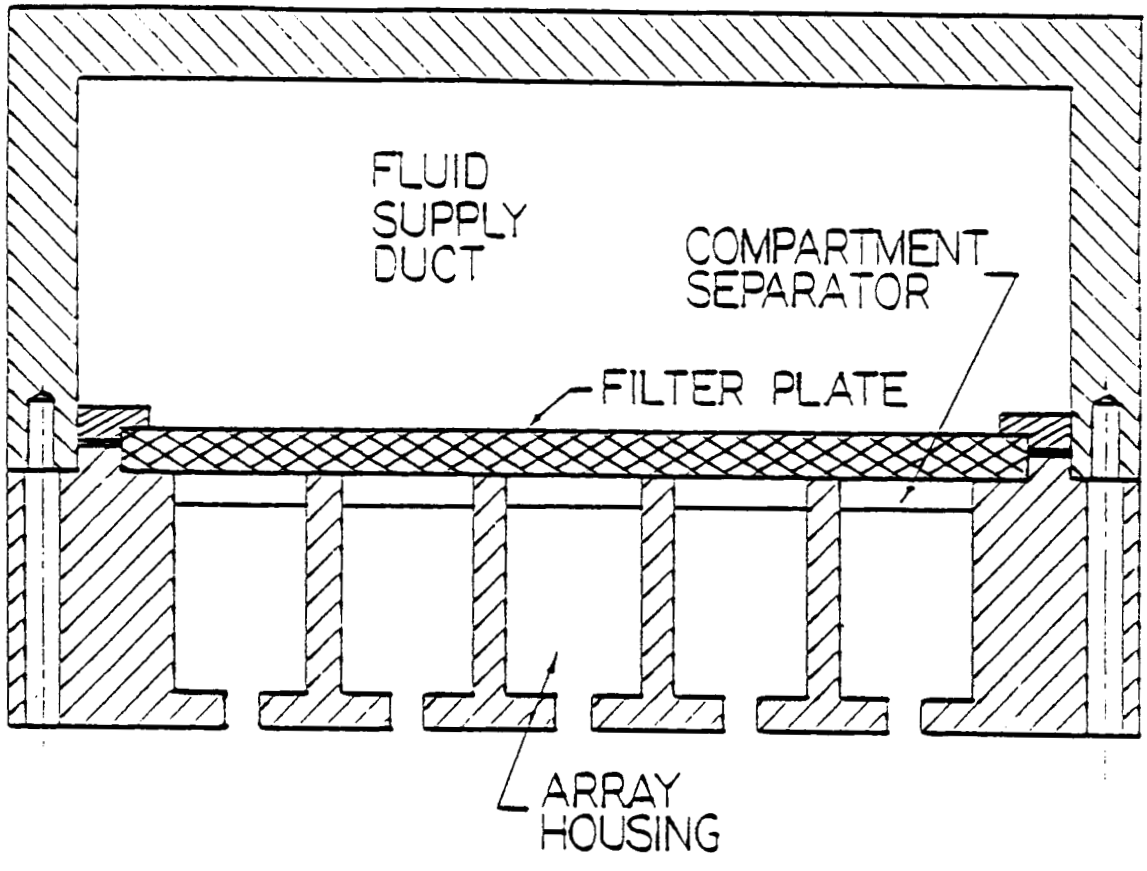

Figure 32: End cross-section view of assembled generator.

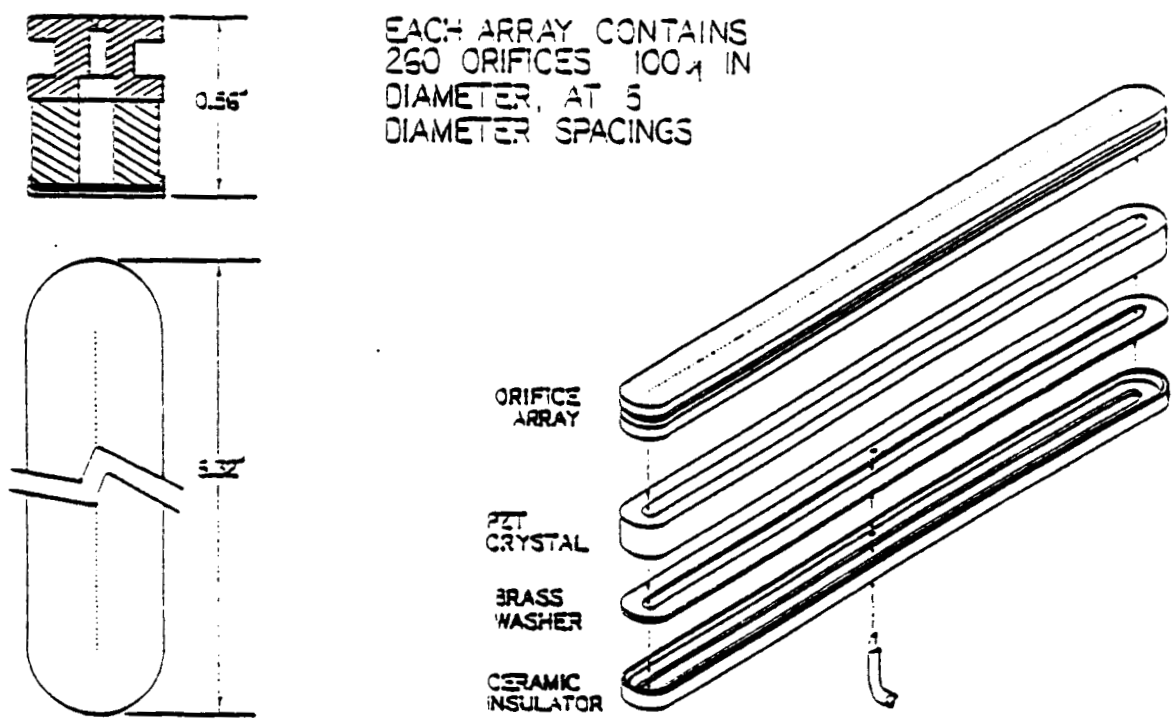

Figure 33: Schematic of orifice array assembly.

NASA
National Aeronautics and Space Administration

Report Documentation Page

1. Report No.	2. Government Accession No.	3. Recipient's Catalog No.
NASA CR-182246		

4. Title and Subtitle
Design and Performance of a Droplet Generator Module for the Liquid Droplet Radiator

5. Report Date
June 1989

6. Performing Organization Code

7. Author(s)
E.P. Muntz, Melissa Orme, Tony Farnham

8. Performing Organization Report No.

10. Work Unit No.
506-41-51

9. Performing Organization Name and Address
University of Southern California
Department of Aerospace Engineering
Los Angeles, California 90089-1191

11. Contract or Grant No.
NAS3-25068

13. Type of Report and Period Covered
Contractor Report Final

12. Sponsoring Agency Name and Address
National Aeronautics and Space Administration
Lewis Research Center
Cleveland, Ohio 44135-3191

14. Sponsoring Agency Code

15. Supplementary Notes
Project Manager, K. Alan White, Power Technology Division, NASA Lewis Research Center
(216) 433-6165

16. Abstract

A pre-prototype segment of a droplet sheet generator for a liquid droplet radiator has been designed, constructed and tested. The ability to achieve a uniform, non-diverging droplet sheet is limited by manufacturing tolerances on nozzle parallelism. For an array of 100, 100 μm dia. nozzles spaced 5 stream diameters apart, typical standard deviations in stream alignment were ± 10 mrad. The drop to drop fractional speed variations of the drops in typical streams were similar and independent of position in the array. The absolute value of the speed dispersion depended on the amplitude of the disturbance applied to the stream. A second generation preliminary design of a 5200 stream segment of a droplet sheet generator has been completed. The design is based on information developed during testing of the pre-prototype segment, along with the results of an acoustical analysis for the stagnation cavity pressure fluctuations used to break-up the streams into droplets.

17. Key Words (Suggested by Author(s))	18. Distribution Statement
Droplet Generator Liquid Droplet Radiator Cavity Acoustics	Unclassified - Unlimited Subject Categories 20,34

19. Security Classif. (of this report)	20. Security Classif. (of this page)	21. No of pages	22. Price*
Unclassified	Unclassified	65	A04

NASA FORM 1626 OCT 86

*For sale by the National Technical Information Service, Springfield, Virginia 22161